DANISH
TECHNOLOGICAL
INSTITUTE

Test rooms for test of PowerShades

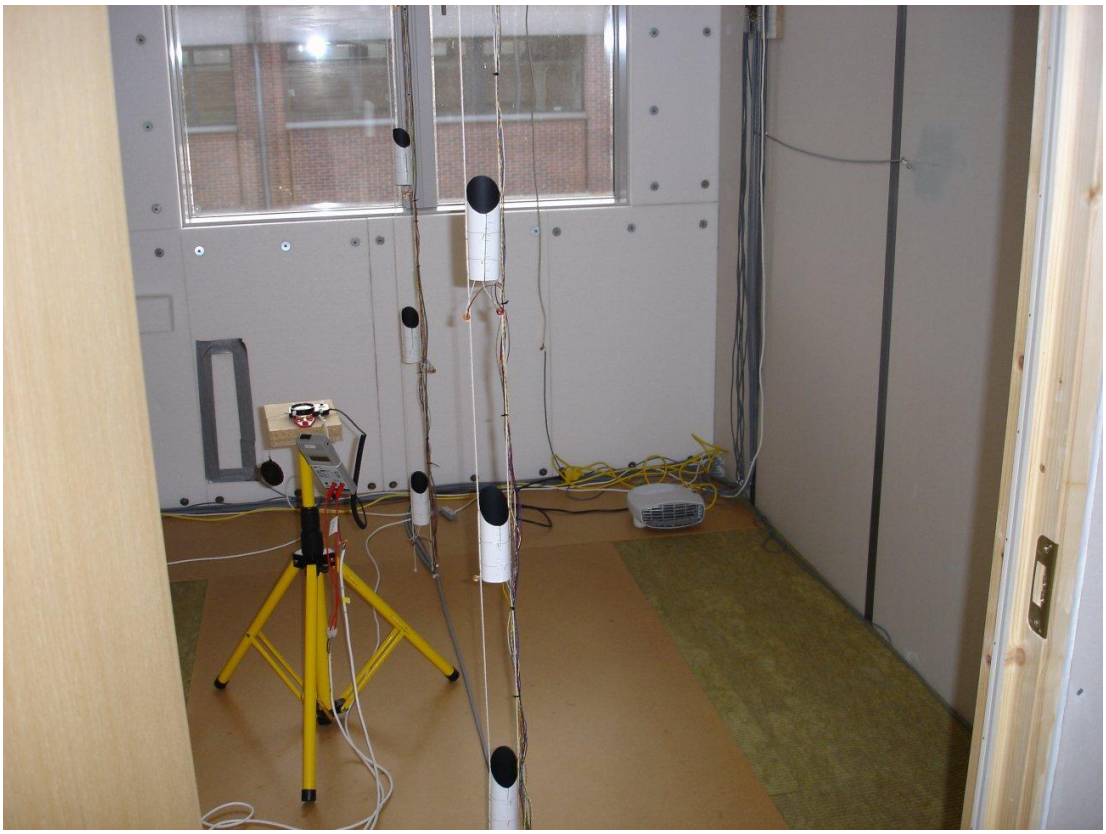

Technological Insitute

Test rooms for test of PowerShades

Søren Østergaard Jensen
Centre for Refrigeration and Heat Pump Technology
Technological Institute

May 2008

Preface

This report describes two test rooms erected for testing PowerShades under realistic conditions. The work performed is part of the project "PowerShades – Development and pilot demonstration of new transparent photo voltaic module" project no. 2006-1-6322 financed by Energinet.dk.

The following persons has participated in the erection and monitoring of the two test rooms:

Søren Østergaard Jensen, M.Sc. Danish Technological Institute
Lars Molnit, B.Sc. Danish Technological Institute
Ole Larsen. OL-Teknik
Eik Bezzel. PhotoSolar

Test rooms for test of PowerShades
1st printing, 1st edition, 2008

Industry and Energy division

ISBN: 87-7756-769-2
ISSN: 1600-3780

List of contents

1. Introduction

PowerShades consist of an opaque solar cell material with holes which partly lets the solar radiation through. Dependent on the design of the holes direct solar radiation from specific incidence angles can be screened off while solar radiation from other directions are allowed to pass as shown in figure 1.1. The PowerShades are aimed to be installed in the glazing of traditional windows.

PowerShades will typically be designed to shade off the direct solar radiation during midday when the sun is high in the sky and when the risk of overheating of the building due to solar radiation is high. Figure 1.2 shows an example of the progressive shading due to PowerShades.

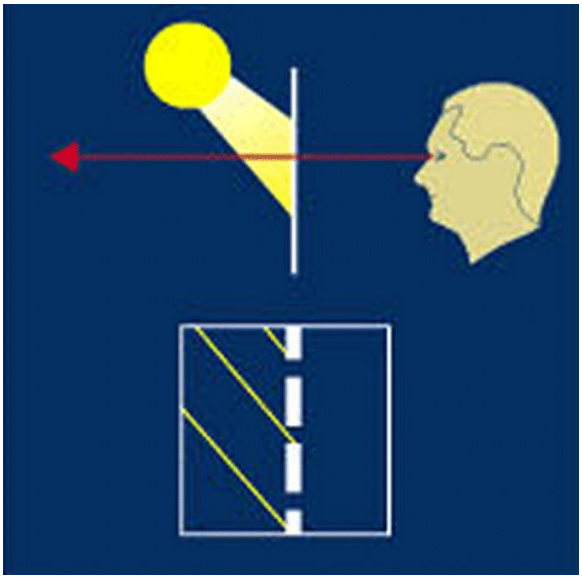

Figure 1.1 The principle of the solar shading feature of PowerShades.

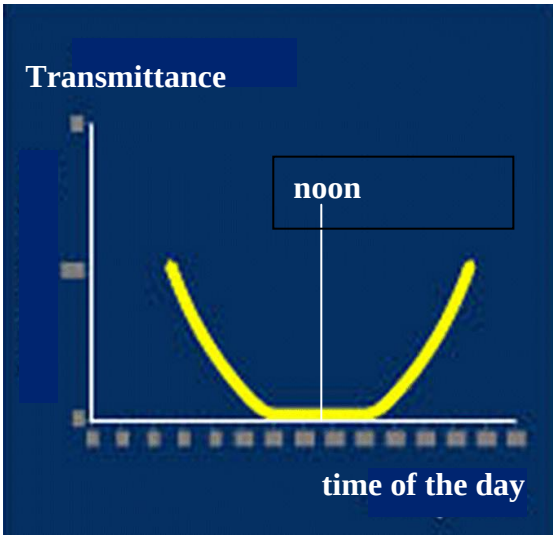

Figure 1.2 Progressive solar shading of direct solar radiation over the day due to the angle selectivity of the PowerShades.

PowerShades were theoretically investigated in the project "Transparent solar cells – the electricity producing solar shading of the future" (Technological Institut, 2005). The thermal behaviour of PowerShades was investigated using the simulation program ESP-r (ESRU, 2001). A new module for dealing with the angle selectivity of PowerShades was developed for ESP-r. ESP-r was used to investigate different designs of PowerShades and to compare the thermal behaviour of PowerShades with traditional forms of solar shading. A building with PowerShades in the south facing windows weas modelled. Further the simulations were carried out for three locations in Europe: Copenhagen (DK), Munich (D) and Palermo (I).

The conclusion from the simulations was that PowerShades perform better than solar shading glass (with a g-value of 0.35) and as well as a highly efficient external shading (with an overall g-value of 0.17). However, these results are based on simulations using a novel module of ESP-r including calculated optical properties of the PowerShades. There was, therefore, a need for verification of the simulation model using measurements from a building with PowerShades mounted in the windows and exposed to real weather conditions.

Simulations and measurements could be compared for PowerShades mounted in real buildings. This will give a good subjective impression of the performance of PowerShades – and this will be done as part of the project. But for purpose of verification of a computer model real buildings are too undefined and uncontrolled. The uncertainty of the measurements is far too high to be used for verification of a model. There is a need for a much more well defined, well controlled yet realistic environment for test of the PowerShades.

Based on the experience from the PASSYS project (Jensen et al, 1994) it was decided to go for side-by-side comparison using test rooms. The following chapters describe the erection of two test rooms at Technological Institute, the thermo-physical and optical properties of the test rooms and the monitoring system for obtaining the necessary measuring data.

2. The test rooms

It was decided to erect 2 test rooms in order to be able to perform a side-by-side comparison. Even using extremely well defined test rooms where all properties are known with a very low uncertainty it is difficult to simulate identical values to those measured. There will always be rather large uncertainties on both measurements and simulations – especially on the latter as a computer model although very details always will be a very simple approximation of the reality. It is thus difficult to obtain good agreement on absolute values but much easier to get good agreement on differences. Here are side-by-side comparisons a strong tool as the focus here is not on the absolute values but on the difference in performance of the rooms when having e.g. different glazing in the windows – eg a traditional window compared to PowerShades or two different designs of PowerShades. This means that one is able more precisely to test the models ability to model the specific feature of interest – here the ability to model PowerShades. All other faults and approximation errors not dealing with the PowerShades are either more or less excluded or at least minimized.

The aim of the work described in the present report was to design, erect and instrument two test rooms suitable for obtaining measurements for verification of the PowerShade model in ESP-r.

It is of course expected that good agreement between measurements and simulations will most properly not be obtained from the start. The measurements will, therefore, be used to calibrate the model in order to obtain satisfactory agreement. Once confidence in the model has been achieved the model will be scaled to be used for simulation of PowerShades in real buildings under different conditions – e.g. different weather conditions and utilization of the building.

2.1. Location of the test rooms

The two test rooms are located in a laboratory at the Technological Institute in Taastrup a little West of Copenhagen. Figure 2.1 shows a plan over the Technical Institute with the building hosting the test rooms and an indication of the location of the test rooms within the building. Figure 2.1 shows that the facades of the test rooms are facing nearly south – more precisely 13° from south towards west.

Figure 2.2 shows a principle drawing of the test rooms situated in the laboratory. Test room B shares as shown a wall with the room besides the laboratory hosting the test rooms. Figure 2.3 shows a picture of the laboratory before erection of the test rooms. The door at the back walls (the shared wall of test room B) has been removed, and the doorway closed by materials almost identical to the existing wall – see later.

The aim was to make the two test rooms as identical as possible, and they are except for the following things:

1) the shared wall in room B. This wall is slightly different from the other walls of the test rooms. This will be discussed in chapter 2.2.
2) the rooms are inverted with respect to the façade as shown in figure 2.4. The two windows are identical for the two test rooms, but while in test room A the smallest window that can open is located to the west it is located to the east in test room B. Further the

column between the windows (figure 2.5) will create shading in the morning in test room A and in the afternoon in test room B.

3) due to the building situated to the east of the building with the test rooms - see figures 2.1 and 2.4 - the shading on the facades of the two test rooms is different in the morning at low sun angles.

The above differences will create differences in the measurements for the two rooms, however, the same discrepancies can be created in the simulations, so this should not give raise to major difficulties. When looking solemnly at the measured date the physical differences should be remembers as the observed discrepancies else may give rise to confusion.

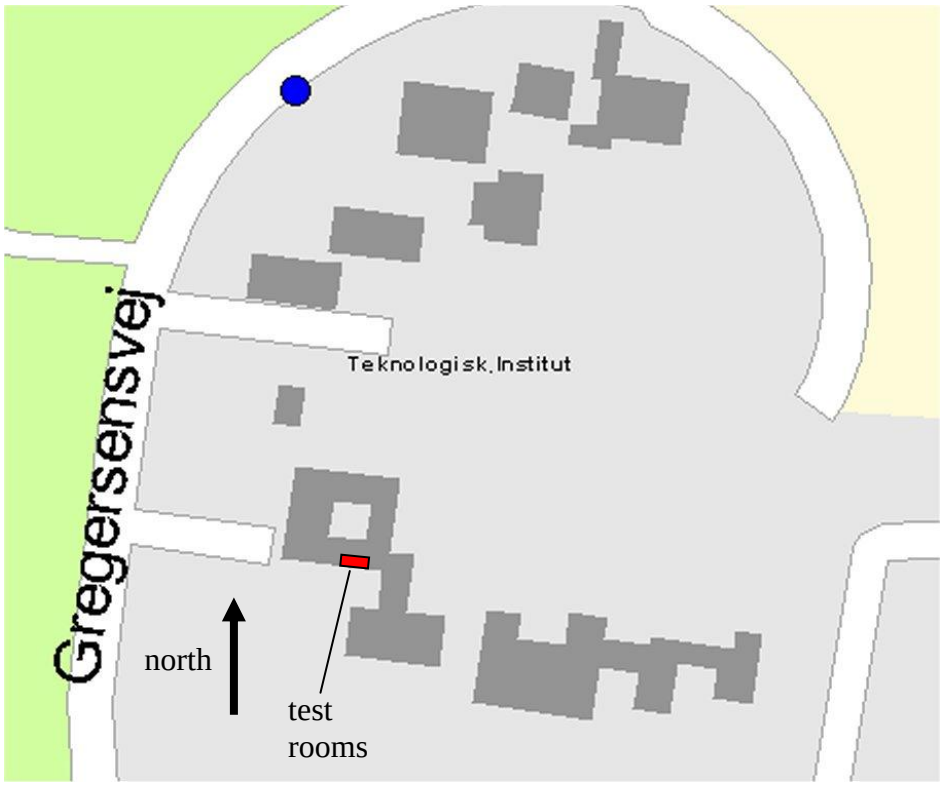

Figure 2.1. The location of the test rooms at the Technological Institute.

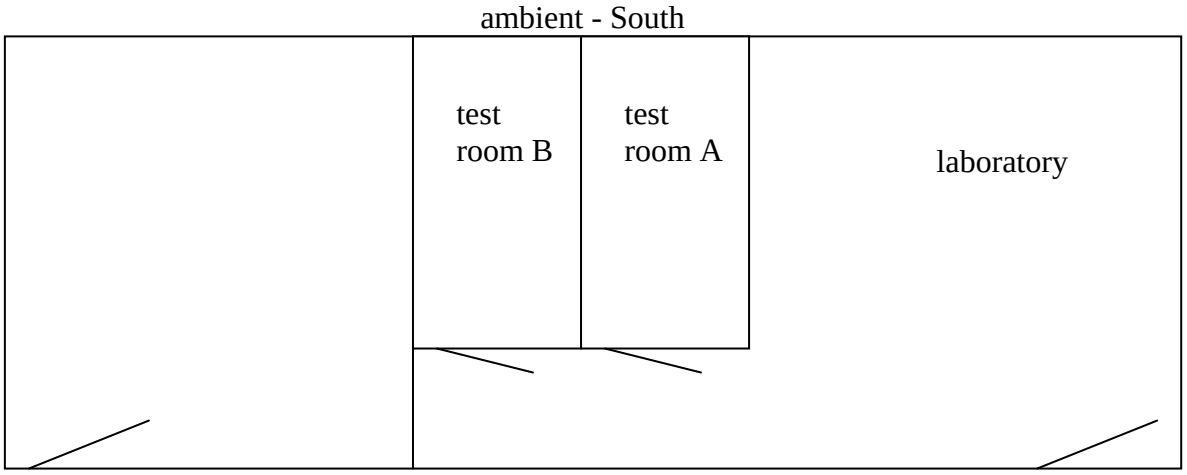

Figure 2.2. Principle drawing of the location of the test rooms within the laboratory.

Figure 2.3. The laboratory before the two test rooms were installed.

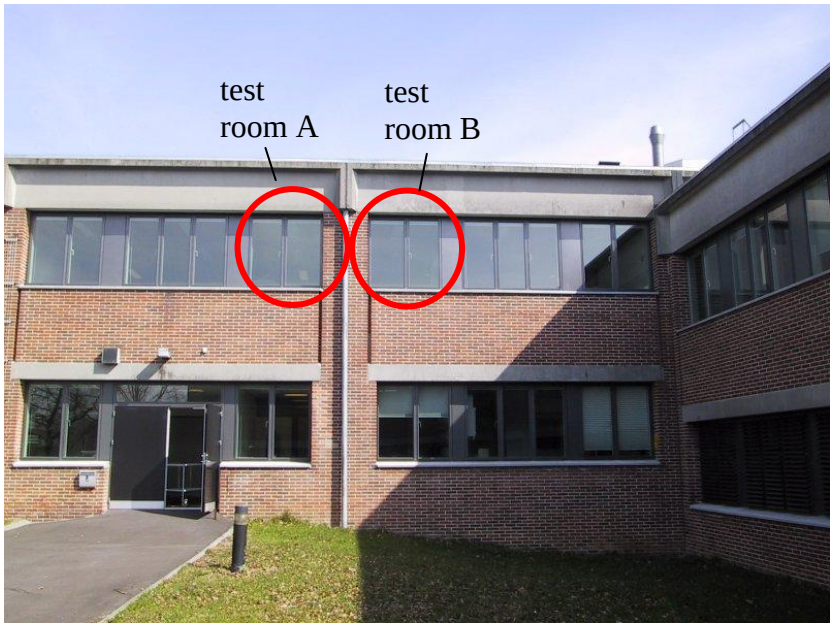

Figure 2.4. Façade of the rest rooms. The red circles show the windows of the two test rooms.

2.2. The dimensions of the test rooms

The dimensions of the two test rooms are almost identical. Figure 2.6 shows the dimensions of the test cells. The internal floor area and volume of the test cells are thus:

	area	volume
Test room A	6.83 m²	16.70 m³
Test room B	6.85 m²	16.76 m³

Figure 2.5. The column in the façade between the two test rooms.

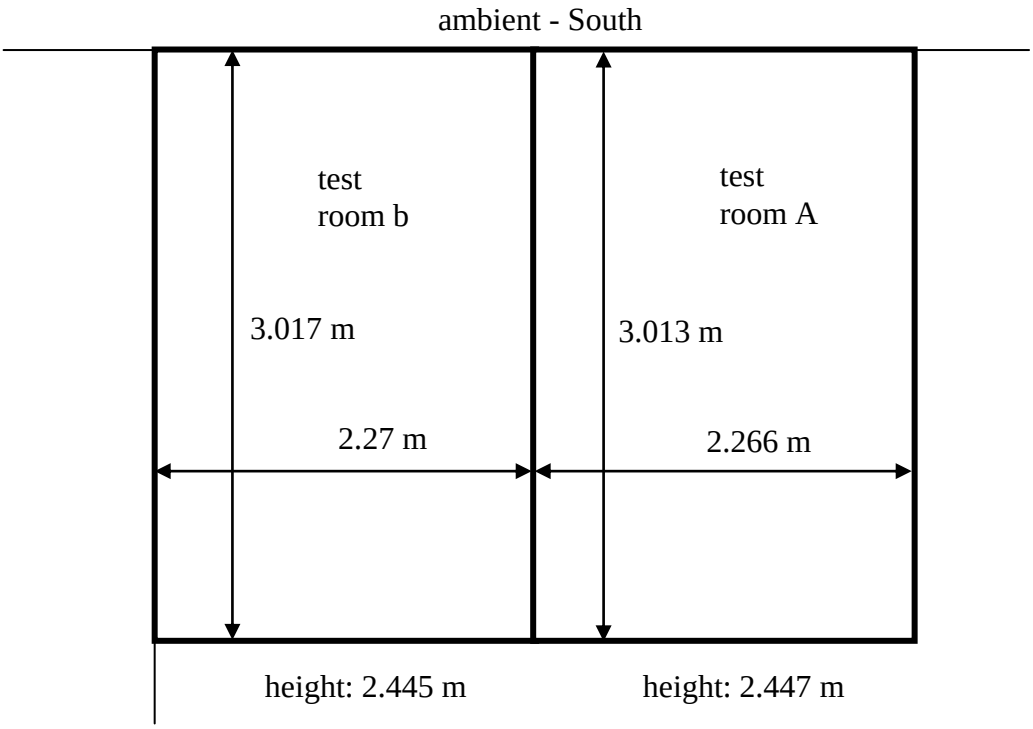

Figure 2.6. The dimensions of the test rooms.

The test rooms are as seen in figure 2.6 almost identical with regards to the dimensions.

2.3. The internal walls of the test room

Expect for the facades the walls of the test rooms consist of a skeleton of thin U-shaped steel bars (sectional bars) - as shown in figures 2.7-8 - with one 12.5 mm A1 gypsum plates from Danogips on each side and 70 mm mineral wool (Flexi A-Batts from Rockwool) between the gypsum plates (figure 2.9).

The sectional bars are made of 0.56 mm steel. The two walls without a door were constructed with 5 vertical bars and two horizontal bars (one on the floor and on at the ceiling) as seen in figure 2.7. The two wall with the entrance door to the test rooms were constructed with 4 vertical bars and two horizontal sectional bars (one on the floor and on at the ceiling) as also seen in figure 2.7. Further two vertical and one horizontal sectional bars are situated above the doors as seen in figure 2.10. Wooden laths were installed in the bars at to doorways to support the door cases as seen in figure 2.8.

Figure 2.11 shows the construction of the shared wall in test room B. The wall is as the other internal walls of the test rooms made of a skeleton of sectional bars but with two 12.5 mm gypsum plates on each side. The shared wall in room B is informed to have one bar per 60 cm. The space between the gypsum plates are filled with 50 mm possible not too well located mineral wool as seen in figure 2.11.

There is a wooden lath at each side of the now closed doorway. The opening area was 0.9 x 2.1 m². The doorway was closed by mounting sectional bars all around the perimeter of the doorway. Two gypsum plates were mounted on each side with 50 mm mineral wool (Flexi A-Batts from Rockwool) in between. Figure 2.12 shows the doorway after sealing.

Figure 2.7. The steel skeleton of the two test rooms.

Figure 2.8. Close up of the sectional bars of the skeleton.

Figure 2.9. One wall after insulation and the gypsum plates being mounted.

Figure 2.10. Sectional bars mounted at each side of the field above the entrance doors of the test rooms.

Figure 2.11. The construction of the shared wall in room B – top of the doorway before closing.

Figure 2.12. The doorway in the shared wall in test room B after closing.

All joints and corners have been sealed with sealing pasta or tape in order to decrease the infiltration of air in and out of the test rooms. This is shown in figure 2.13.

Figure 2.13. Sealing of joints and corners.

Data on the materials of the internal walls

Steel bars:	thickness	0.56 mm
	thermal conductivity:	60 W/mK
	thermal capacity:	480 J/kgK
	density:	7860 kg/m³
Mineral wool:	thickness	70 mm and 50 mm
	thermal conductivity:	0,037 W/mK
	thermal capacity:	2700 J/kgK
	density:	28.5 kg/m³
Gypsum plates:	thickness	12.5 mm
	thermal conductivity:	0.18 W/mK
	thermal capacity:	1090 J/kgK
	density:	720 kg/m³
Laths in new doorways:	dimensions	57 x 37 mm
	thermal conductivity:	0.125W/mK
	thermal capacity:	2100 J/kgK
	density;	437 kg/m³
Laths in old closed doorway:	dimensions	57 x 37 mm
	thermal conductivity:	0.125W/mK
	thermal capacity:	2100 J/kgK
	density;	437 kg/m³

The above data has been used to generate the input data for the simulation model – se chapter 2.8.

2.3.1. The doors in the internal walls

The entrance doors to the test rooms have an overall hole in the walls of 0.9 x 2.1 m² and an actual opening area of 0.805 x 2.02 m². The doors have an area of 0.82 x 2.04 m². The doors have a frame made of chip board. The frame is covered with 3.5 mm plywood. How the distance between the two sheets of plywood is maintained is not known. The door cases are made of wood. The U-value of the doors is estimated to be around 3 W/m²K.

In order to maintain only little infiltration sealing strips are located all around the perimeter of the door as seen in figure 2.14.

As it is very difficult to calculate the overall U-value of the door incl. door case an internal insulated "door" has been produced to fit into the door case but else laying close to the wall around the door. The internal door are made of 4 mm plywood facing the traditional door and 50 mm polystyrene foam (ESP 80 Standard from Thermisol) plates facing the test room as seen in figure 2.15. The internal door is has a dimension of 1 x 2.11 (from the top of the insulation on the floor) m² in order to also cover the door case of the internal wall. In order to de-

crease the infiltration with the surrounding laboratory sealing strips are located between the wall and the internal door all the way round the door except at the floor.

Figure 2.14. The entrance door of one of the test rooms.

Figure 2.15. The internal door of the test rooms. To the left seen from the outside and to the right from the inside.

Data on the materials of the internal doors

Plywood:	thickness	3.9 mm
	thermal conductivity:	0.165W/mK
	thermal capacity:	2100 J/kgK
	density;	661 kg/m³
Polystyrene:	thickness	50 mm
	thermal conductivity:	0.038W/mK
	thermal capacity:	1400 J/kgK
	density:	16 kg/m³

Space between the doors and the internal doors: 42 mm

The above data has been used to generate the input data for the simulation model – se chapter 2.8.

2.4. The external wall of the test room

The external walls of the test rooms are the original façade from the start of the 70'ties. The original façade is rather complex as figures 2.16-18 show. Figures 2.16-17 show vertical and horizontal sectional drawings of the original external wall of the test rooms, while figure 2.18 shows pictures of the inside of the original wall. The windows (see chapter 2.4.1) are new – replaced during 2005. In order to ease the modelling of the façade 50 mm of foam insulation (ESP 80 Standard from Thermisol) were mounted on the inside of the external wall as seen in figure 2.19. Figure 2.20 shows at close up of the insulation foam at the window frame. The small bulge to the left under the window is due to the wiring box seen to the right under the window in figure 2.13.

The original external wall is very difficult to model due to the complexity of it. By adding extra internal insulation the thermal properties of the materials of the original wall become less important to know precisely. The polystyrene plates were mounted by means of 46 3.5 mm steel screws. This increases the overall thermal conductivity of the insulation foam. This has been accounted for in the input data for the simulation program in chapter 2.8.

Data on the materials of the external walls

Bricks - internal:	thickness	0.108 mm
	thermal conductivity:	0,56 W/mK
	thermal capacity:	1000 J/kgK
	density:	1650 kg/m³
Bricks - external:	thickness	0.108 mm
	thermal conductivity:	0,667 W/mK
	thermal capacity:	1000 J/kgK
	density:	1650 kg/m³
Mineral wool:	thickness	100 mm
	thermal conductivity:	0,037 W/mK

	thermal capacity:	2700 J/kgK
	density:	28.5 kg/m³
Concrete - internal:	thickness	changing
	thermal conductivity:	2.44 W/mK
	thermal capacity:	1000 J/kgK
	density:	2200 kg/m³
Concrete - external:	thickness	changing
	thermal conductivity:	2.54 W/mK
	thermal capacity:	1000 J/kgK
	density:	2200 kg/m³
Fibre board:	thickness	12 mm
	thermal conductivity:	0.17W/mK
	thermal capacity:	2100 J/kgK
	density:	900 kg/m
Wood:	dimensions	changing
	thermal conductivity:	0.125W/mK
	thermal capacity:	2100 J/kgK
	density;	437 kg/m³
Polystyrene:	dimensions	50 mm
	thermal conductivity:	0.038 W/mK
	thermal capacity:	1400 J/kgK
	density:	16 kg/m³
Screws:	dimensions	ø3.5mm
	thermal conductivity:	60 W/mK
	thermal capacity:	480 J/kgK
	density:	7860 kg/m³

The above data has been used to generate the input data in for the simulation model – se chapter 2.8.

Figure 2.18. Pictures of the inside of the original external wall.

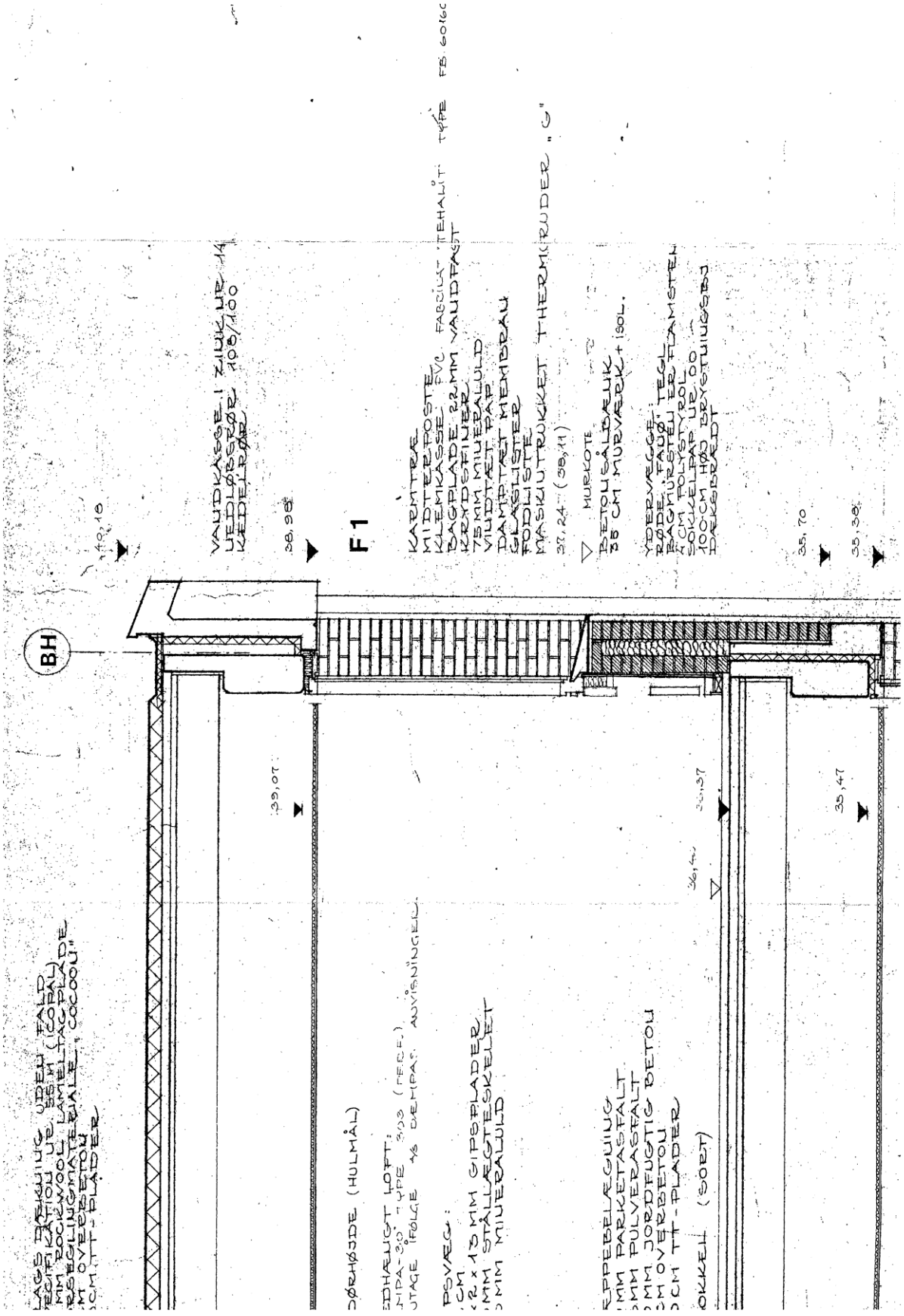

Figure 2.16. Vertical sectional drawing of the original external wall

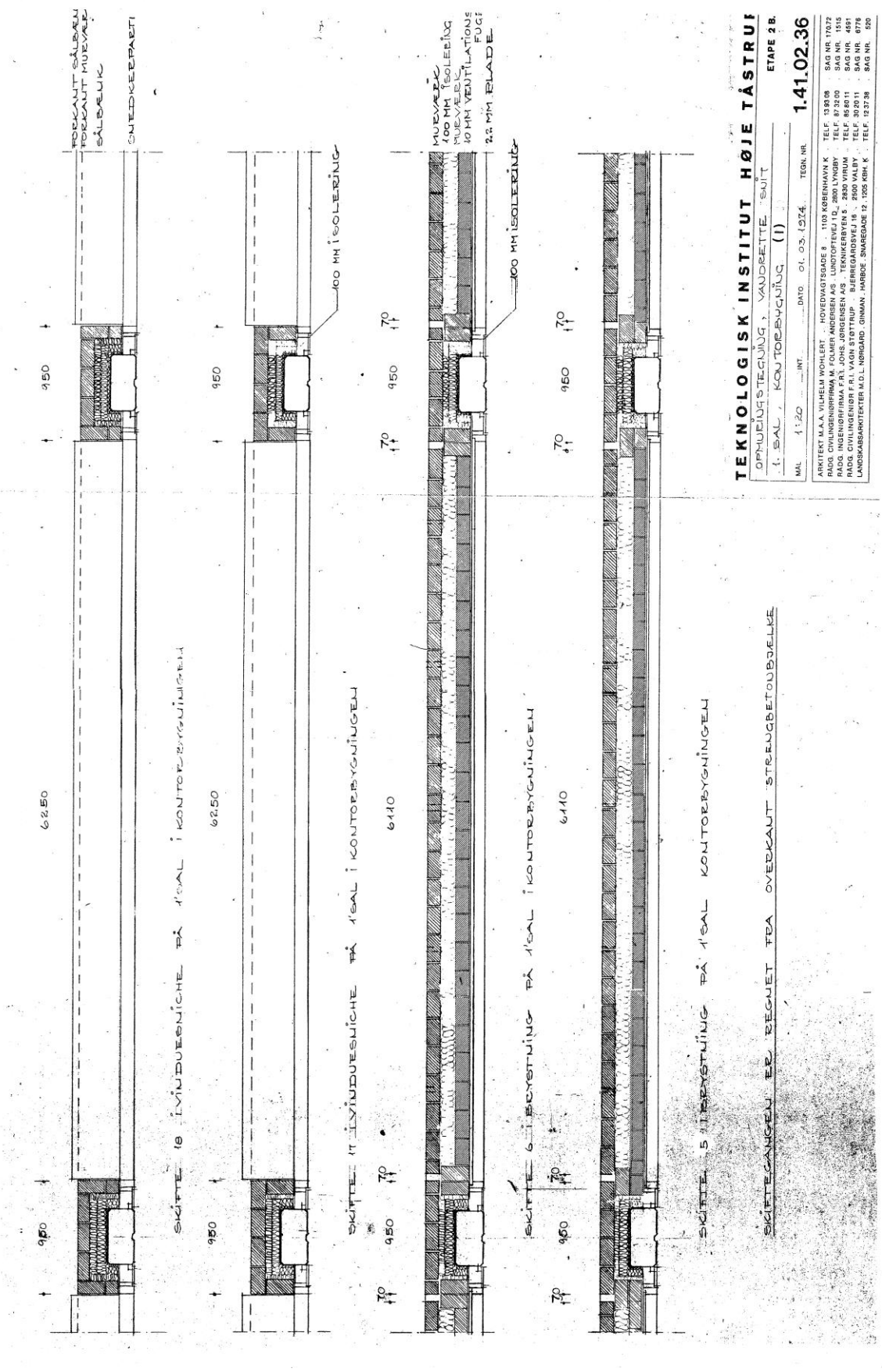

Figure 2.17. Horizontal sectional drawings of the original external wall.


Figure 2.19. Pictures of the inside of the facades after insulation with insulation foam plates.

Figure 2.20. Close up of the insulation foam at the window frame.

2.4.1. The original windows of the test room

The windows from the 70'ies were in 2005 replaced with new windows from the Danish firm Velfac. As the products at Velfac are traceable it was easy to obtain the necessary properties of the windows

The windows in the two test rooms are identical. The windows consist in each test room of two slightly different window pans mounting in a common frame with a bar between the two window pans as seen in figure 2.19. The smaller of the windows can be opened while the large is fixed. The hole in the wall is 1.57 x 1.58 = 2.48 m², while the total transparent area is 1.98 m²

Velfac gives the following properties for the windows (Velfac sun 1/clear):

Outside 6 mm glass with low e-coating, cavity of 14 mm filled with Argon and inside 4 mm glass.

Centre U-value for the glazing:	1.1 W/m²K
U-value for the framing:	3.1 W/m²K
Edge loss coefficient between glazing and framing:	0.058 W/mK

Optical properties:

Light transmission:	67 %
Light reflectance	
outside:	11 %
inside:	12 %
UV-transmittance:	5 %
Solar direct transmittance:	34 %
Solar direct reflectance:	31 %
Solar direct absorptance	
outside pane:	34 %
inside pane:	1 %
Solar factor:	37 %

Thermal properties of the frame

Thermal conductivity:	0.13 W/mK
Thermal capacity:	1600 J/kgK
Density:	500 kg/m³

2.5. The ceiling of the test rooms

The roofing of the laboratory is as the external wall rather complex, and further ductworks, tubes and wiring is situated below the ceiling. It was, therefore, decided to replace the original suspended ceiling (see figure 2.16) with a new ceiling forming the ceiling of the test rooms. In this way the materials of the ceiling would be well known and instead of measuring the ambient temperature above the roof, the temperature of the air space between the ceiling of the test rooms and the ceiling of the laboratory should be measured. In this way more precise measurements can be obtained as the influence of solar radiation and long wave radiation to the sky is eliminated.

The ceiling of the test rooms were constructed by suspending wooden boards (95 x 22.5 mm²) across the laboratory per each 600 mm as seen in figure 2.21. Underneath the wooden boards an unbroken piece of plastic foil were mounted in order to secure air tightness of the ceiling – figure 2.21. The plastic foil was taped to the walls in order to minimize the infiltration along the edges. Underneath the plastic foil 50 mm of polystyrene foam plates identical to the ones used at the façade (ESP 80 Standard from Thermisol) were mounted as seen in figure 2.22. Identically to the façade the foam plates were mounted using 3.5 mm screws – in total 64 screws in test room A and 62 in test room B. This increases the overall thermal conductivity of the insulation foam. This has been accounted for in the input data for the simulation program in chapter 2.8.

Figure 2.21. The wooden boards and plastic foil forming the top of the ceiling in the test rooms.

Figure 2.22. Mounting the insulation foam plates at the ceiling of the test rooms.

Data on the materials of the ceiling

Polystyrene:	thickness	50 mm
	thermal conductivity:	0.038 W/mK
	thermal capacity:	1400 J/kgK
	density:	16 kg/m³
Screws:	dimensions	ø3.5mm
	thermal conductivity:	60 W/mK
	thermal capacity:	480 J/kgK
	density:	7860 kg/m³

2.6. The floor of the test rooms

The floor is made of concrete T-bars with at topping of linoleum, asphalt and concrete. The properties of the floor are not well known. Further in order to decrease the influence of the uncertainty of the temperatures measurements in the test rooms on the simulations, there is a wish of generating of large temperature difference between the room with the existing window and the room with PowerShades. For both above reasons insulation was situated on top of the floor as seen in figure 2.23. 50 mm casting mineral wool batts (Terrænbatts Erhverv Floor-to-ground slab) were situated on top of the original floor. In order to be able to work in the test rooms 3 mm hard fibre boards were located on top of the insulation as seen in figure 2.24. The hard fibre boards cover 62 % of the floor area of the test rooms. A temperature sensor has been located under the casting mineral wool – see chapter 3 – so that the properties of the original floor do not need to be known nor the temperature of the room below.

Figure 2.23. Insulation of the floor of the test rooms.

Data on the materials of the floor

Hard fibre board:	thickness	3 mm
	thermal conductivity:	0.17 W/mK
	thermal capacity:	2100 J/kgK
	density:	900 kg/m³
Mineral wool:	thickness	50 mm
	thermal conductivity:	0,038 W/mK
	thermal capacity:	2700 J/kgK
	density:	100 kg/m³

The above data has been used to generate the input data for the simulation model – se chapter 2.8.

Figure 2.24. A hard fibre boards are located on the top of the floor insulation.

2.7. Air tightness of the test room

Effort has as described in the previous chapters been made to make the test rooms as air tight as possible. However, some infiltration may still occur between the two test rooms, between the test rooms and the surrounding rooms and between the test rooms and ambient. In order to be able to calibrate the computer model it is important to know the magnitude of the infiltration so that this can be accounted for in the model.

In order to determine the infiltration the technique of passive tracer gas has been utilized. The infiltration measurements were performed by the Danish Building Research Establishment. The method is described in (Bergsøe, 1992).

2.8. Input data to the simulation model

Based on the above description of the test rooms input data for a simulation program has been generated.

2.8.1. Dimensions

The dimensions in figure 2.6 are used.

2.8.2. Material properties

The following input data are necessary for the simulation program ESP-r:

- thermal conductivity
- density

- specific heat
- thickness of layer
- inside surface emissive
- outside surface emissive
- inside surface solar absorptivity
- outside surface solar absorptivity

It is not an easy task to obtain the above parameters for all the materials used in the test rooms. Some of the following parameters are obtained from the manufactures, some from handbooks others are measured values e.g. densities and the solar absorptance found by measuring the reflectance. The latter has been done for the gypsum plates, the hard fibre board, the hard mineral wool (on the floor) and the polystyrene – ie. all the major internal surfaces of the test rooms.

Internal wall

The insulation layer of the internal walls is not homogeneous due to the steel bars. Based on fined element calculations mean values have been calculated for this layer – see figure 2.25. The existing internal wall to the other laboratory is calculated with an air gap on each side of 50 mm insulation – and two gypsum plates on each side.

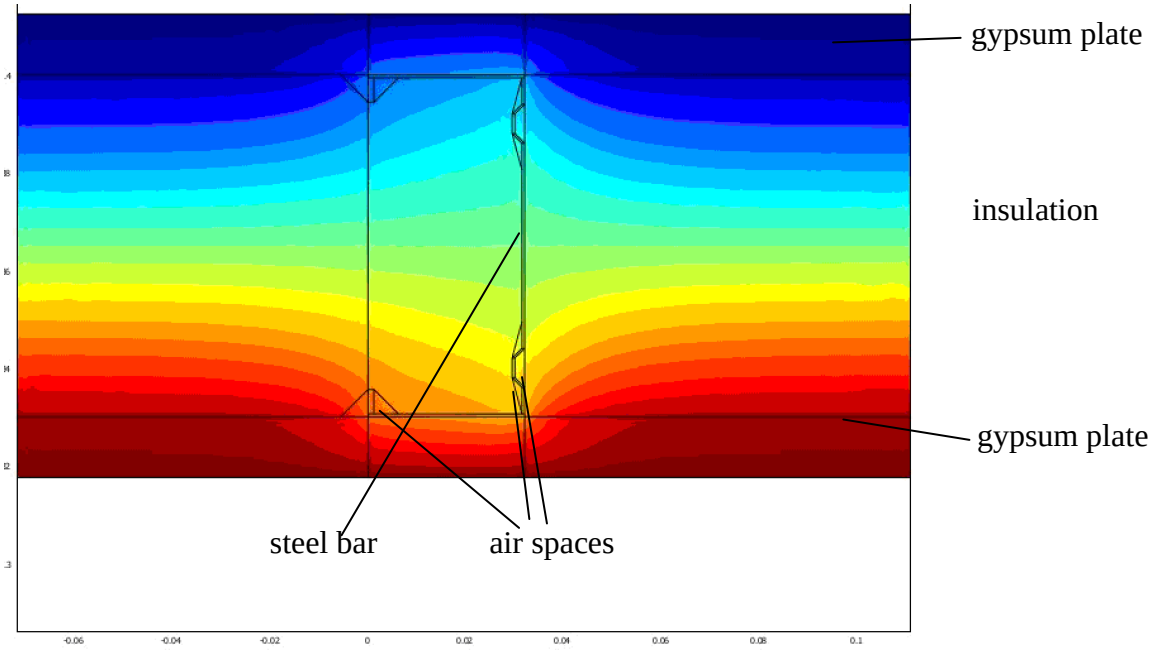

Figure 2.25. Isotherms in internal wall in a piece around the steel bar.

Layer	thermal conductivity W/mK	density kg/m³	specific heat J/kgK	thickness m
gypsum	0.18	720	1090	0.0125
mineral wool 70 mm	0.051	39.3	2701	0.07
mineral wool 50 mm	0.074	31.5	2216	0.07
gypsum	0.18	720	1090	0.0125

Inside surface emissive: 0.94
Outside surface emissive: 0.94
Inside surface solar absorptivity: 0.44
Outside surface solar absorptivity: 0.44

Doors in the test rooms

The real door is assumed to have a U-value of 3 W/m²K. This has been transformed to at equivalent thermal conductivity. The density has been calculated by weighting of a door.

Layer	thermal conductivity W/mK	density kg/m³	specific heat J/kgK	thickness m
polystyrene	0.038	16	1400	0.05
plywood	0.165	661	2100	0.0039
air space	resistance of 0.16 mK/W			0.042
door	0.12	208	2100	0.04

Inside surface emissive: 0.94
Outside surface emissive: 0.82
Inside surface solar absorptivity: 0.22
Outside surface solar absorptivity: 0.35

Facade of the test rooms

Figures 2.16-17 shows that the existing façade of the test rooms is rather complex. Instead of trying to model the façade in details the façade has been divided into three areas as seen in figure 2.26: the wall, the window pane(s) and the frame of the window.

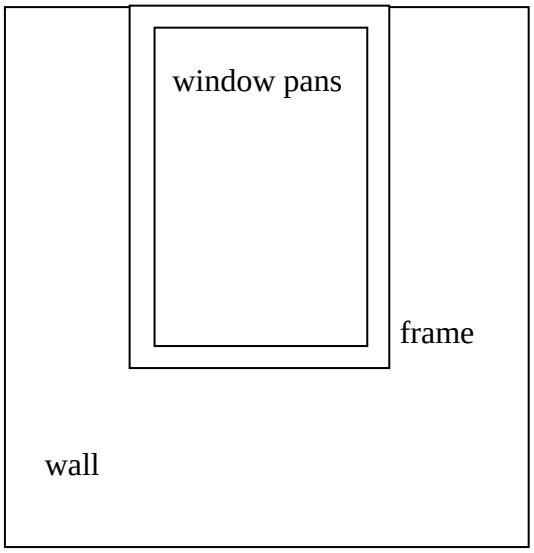

Figure 2.26. The tree areas the façade has been divided into for modelling purposes.

Wall

The wall consists of the original wall and the polystyrene plates. By means of fined element calculations equivalent values for thermal conductivity, density and specific heat has been obtained for the original wall. A larger area than the internal area of the façade has been modelled in order to account for 2- and 3D losses. Figure 2.27 shows the model applied for obtaining the values of the original wall.

Figure 2.27. Fined element calculation of the heat loss through the original walls. To the right isotherms in the parapet.

Due to the screws the thermal conductivity of the polystyrene is somewhat higher. The thermal conductivity is obtained by fined element calculation as shown in figure 2.28. Although the isotherms in figure 2.28 seem rather unaffected by the screws that thermal conductivity is increased from 0.038 to 0.057 W/mK. The density and specific heat is found by weighting between polystyrene and screws.

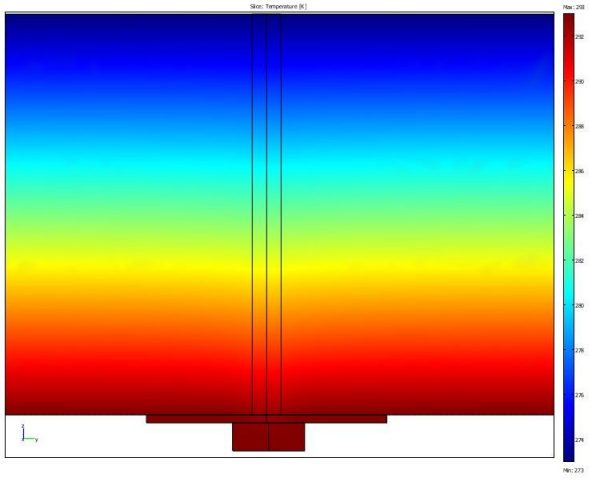

Figure 2.28. Isotherms in a piece of polystyrene foam with a screw.

Layer	thermal conductivity W/mK	density kg/m³	specific heat J/kgK	thickness m	area m²
original wall	0.215	943	1646	0.436	3.065
polystyrene	0.057	17.2	1400	0.05	

Inside surface emissive: 0.94
Outside surface emissive: 0.94
Inside surface solar absorptivity: 0.22
Outside surface solar absorptivity: 0.56

Window frame

Based on the information from Velfac in section 2.4.1 on U-value and edge losses and the measures of the frame the overall U-value of the frame has been calculated to be 4.08 W/mK. The frame is 145 mm thick. The equivalent thermal conductivity is thus 4.08·0.145 = 0,592 W/mK.

Layer	thermal conductivity W/mK	density kg/m³	specific heat J/kgK	thickness m	area m²
window frame	0.592	500	1600	0.145	0.505

Inside surface emissive: 0.93
Outside surface emissive: 0.97
Inside surface solar absorptivity: 0.30
Outside surface solar absorptivity: 0.95

Window panes

The two window panes are as seen in figure 2.25 treated as one pane. This has no influence on the calculations as the edge losses for the real length of edges has been considered above.

The U-value of the window panes is 1.1 W/m²K. The resistance of the air gab has been adjusted to given an overall U-value of W/m²K.

Layer	thermal conductivity W/mK	density kg/m³	specific heat J/kgK	thickness m	area m²
outer glass	0.81	2700	750	0.006	1.98
air gap	resistance of 0.727 mK/W			0.014	
inner glass	0.81	2700	750	0.004	

Inside surface emissive: 0.83
Outside surface emissive: 0.83
Inside surface solar absorptivity: 0.05
Outside surface solar absorptivity: 0.05

Ceiling

Due to the screws the thermal conductivity of the polystyrene is somewhat higher. The thermal conductivity is obtained by fined element calculation as shown in figure 2.28. Although the isotherms in figure 2.28 seem rather unaffected by the screws that thermal conductivity is increased from 0.038 to 0.057 W/mK. The density and specific heat is found by weighting between polystyrene and screws.

Layer	thermal conductivity W/mK	density kg/m³	specific heat J/kgK	thickness m
polystyrene	0.057	17.2	1400	0.05

Inside surface emissive: 0.94
Outside surface emissive: 0.94
Inside surface solar absorptivity: 0.22
Outside surface solar absorptivity: 0.22

Floor

The thickness of the hard fibre board has been reduced to 62% as this board only covers 62% of the floor area.

Layer	thermal conductivity W/mK	density kg/m³	specific heat J/kgK	thickness m
hard fibre board	0.17	900	2100	0.0019
mineral wool	0.038	100	2700	0.05

Inside surface emissive: 0.95
Outside surface emissive: 0.95
Inside surface solar absorptivity: 0.74
Outside surface solar absorptivity: 0.74

2.8.3. Optical properties

The optical values for the original windows is given at an incidence angle of 0°, however, for the model of the test rooms it is necessary to know the optical values at different incidence angles. Velfac cannot give these values. So based on assumptions from other windows the optical values have been generated for other incidence angles than 0°, These values are shown in the table below. The values are shown graphically in figure 2.39. The values at other incidence angles than 0° are uncertain.

Layer	incidence angle °				
	0	40	55	70	80
Total transmittance	0.340	0.360	0.332	0.230	0.056
Absorption in outer glass pane	0.340	0.353	0.365	0.387	0.384
Absorption in inner glass pane	0.010	0.012	0.012	0.011	0.005
Total reflectance	0.310	0.275	0.291	0.372	0.555

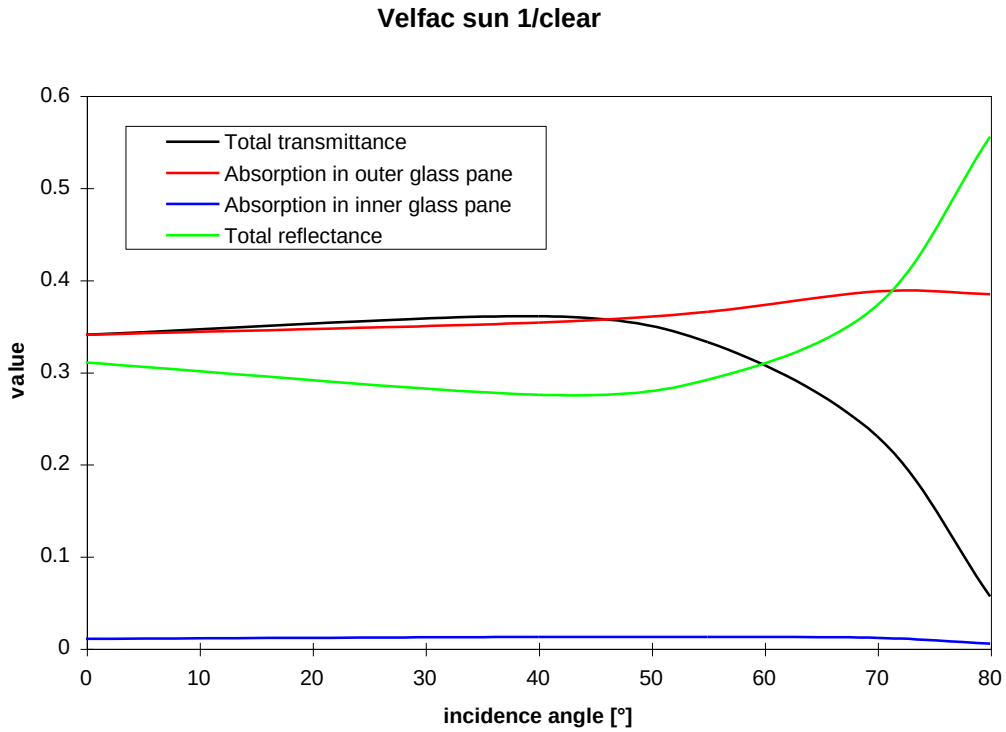

Figure 2.39. Optical properties for the original windows dependent on the incidence angle.

2.8.4. Infiltration

Passive tracer gas measurements were conducted twice with three tracer gasses during the period May 18-24, 2007. However, the measurements remained inconclusive. The Danish Building Establishment couldn't derive the flow rates between the test rooms, between the test rooms at the laboratories and between the test rooms and ambient.

It is therefore judge that the air exchange of the test rooms is insignificant. Also based on the fact that sealing the windows didn't change the result of the measurements. Further the model of the test rooms has been used to introduce infiltrations in the test rooms. The results from these simulations led to results witch were not in accordance with the measurements.

3. Measuring system

The purpose of the test rooms is to investigate the performance of PowerShades both directly as side-by-side comparison and by calibrating a simulation model of the test rooms in order to easily be able to perform parameter studies. However, for both purposes it is necessary to measure the thermal performance of the test rooms and relevant external influences with a high accuracy.

A comprehensive measuring system has thus been installed in and around the test cells. The measuring system is described in details in the following.

Figure 3.1 shows the principle locations of the sensors of the measuring system.

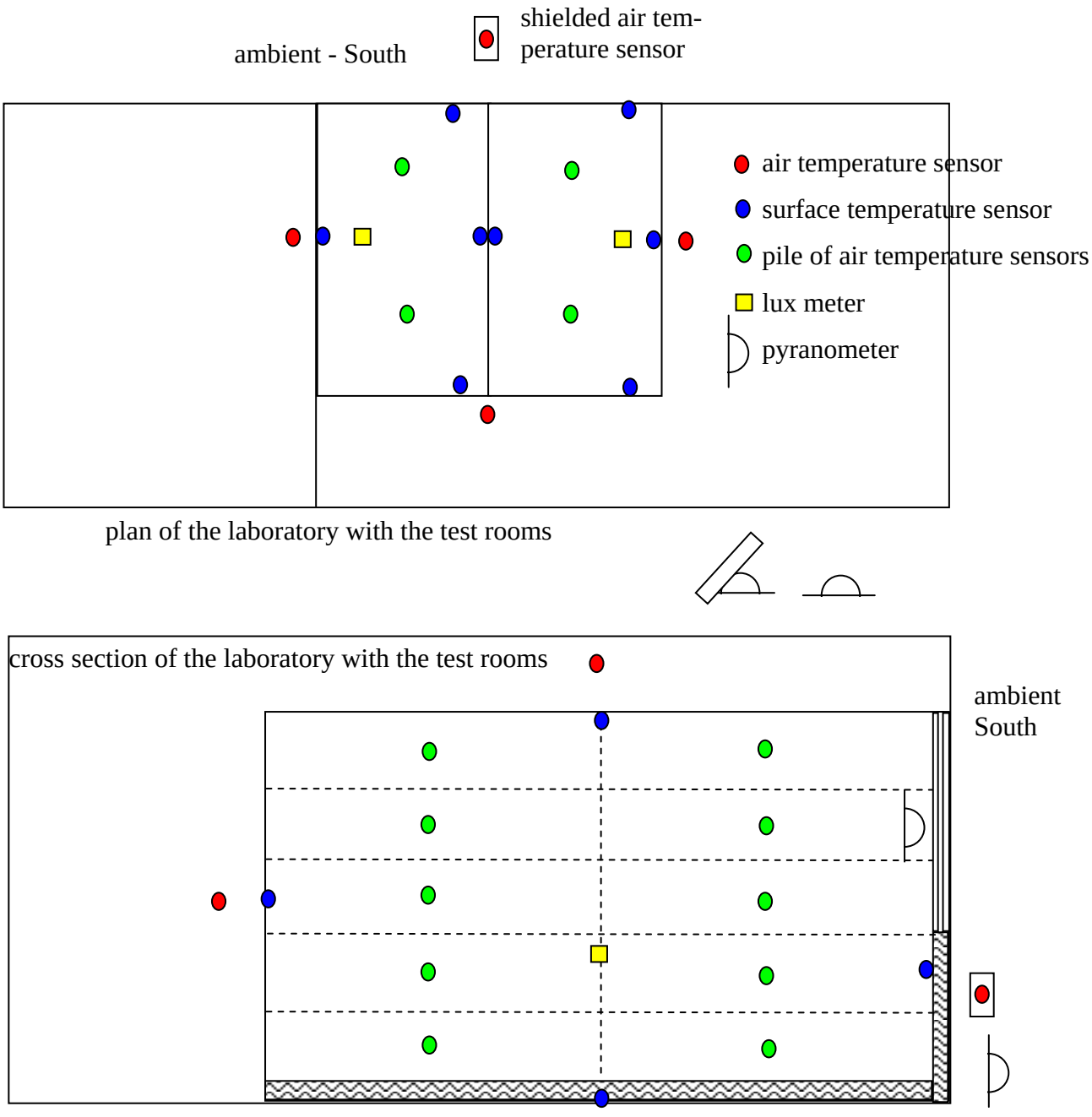

Figure 3.1. The sensors of the measuring system.

3.1. List of sensors

The following list is divided into three groups: temperature sensors, pyranometers and others:

Temperature sensors

20 air temperature sensors in the test rooms – 5 x 2 in each room
12 surface temperature sensors in the test rooms – 6 in each room
6 air temperature sensors around the test rooms – 5 inside and 1 external
2 alarm temperature sensors – one in each room

Pyranometers

2 horizontal pyranometers – one shielded
3 vertical pyranometers – 2 in the test rooms and 1 external
2 vertical pyranometers were later introduced

Others

2 lux meters – one in each room
2 power meters – one for each room

The above sensors are described in details in the following.

3.2. Temperatue sensors

All temperature sensors are PT100 1/3 class B sensors from Jumo with an accuracy of ±0.1 K at 0°C and ±0.27 K at 100°C. This type of PT100 sensors has the lowest uncertainty in the required range.

3.2.1. Air temperature sensors

In order to facilitate the calibration of the simulation model of the test rooms a shielded air temperature sensor has been located in the middle of ten equally sized air volumes of the rooms as seen in figure 3.1 – the rooms has been divided in 5 layers of equal height which again were divided in a front and a back column. This further gives the temperature stratification of the room both horizontally and vertically.

Some of the temperature sensors in test room A are shown in figure 3.2. The sensors were shielded as seen in figures 3.2-3 in order to protect them from being heated by the sun directly. The shields were made of two concentric cylinders as seen in figure 3.3. The shields have limited mass

The air temperature sensors incl. shields were installed in the right position by means of two suspended strings for each pile of air temperature sensors as seen in figure 3.4.

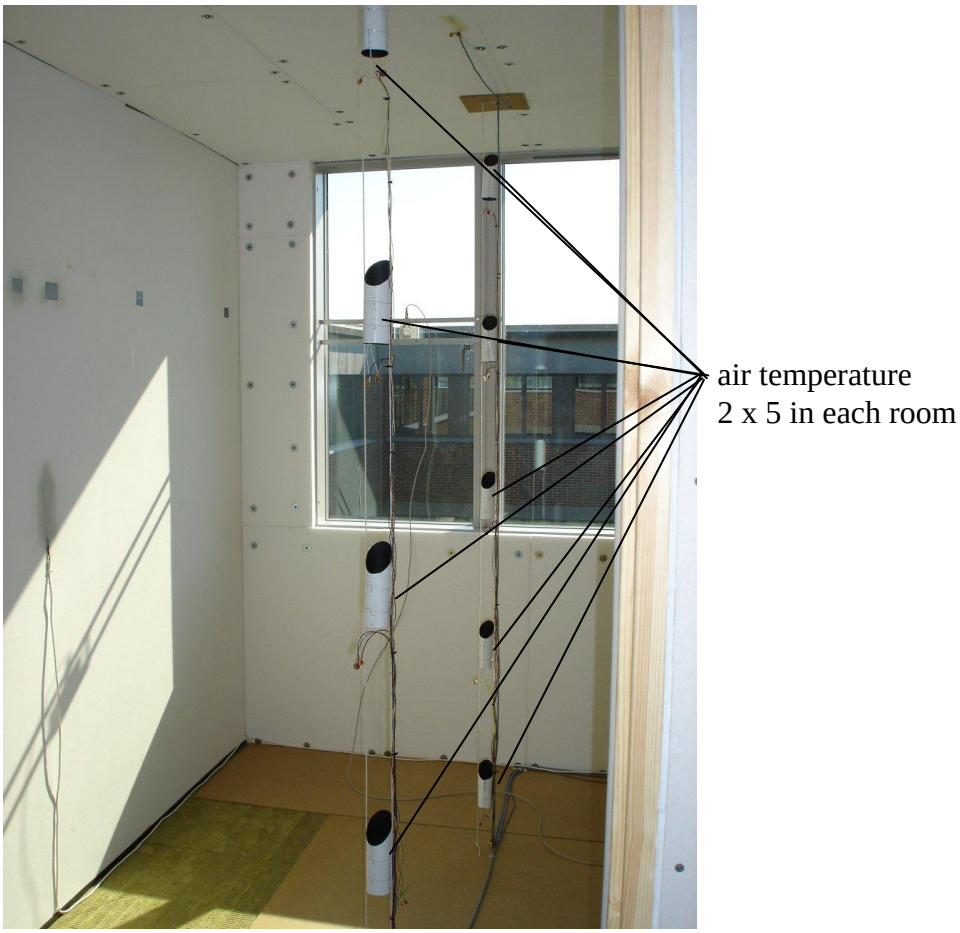

Figure 3.2. 8 of the shielded air temperatures in test room A.

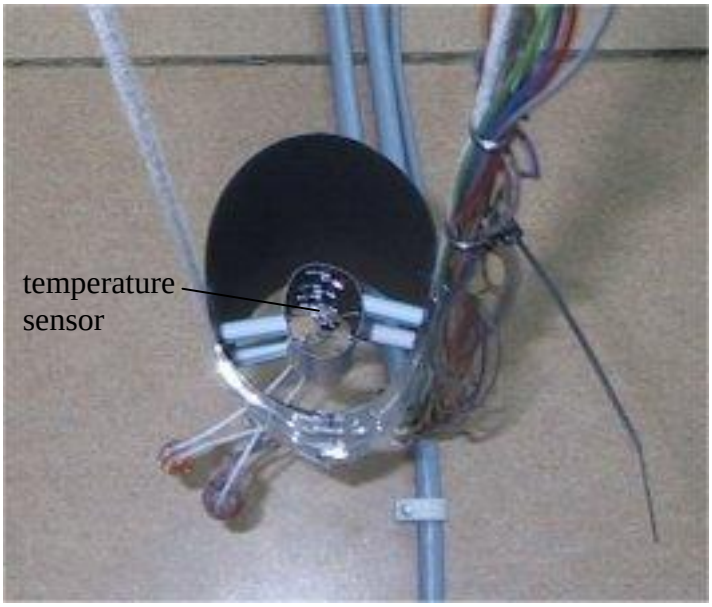

Figure 3.3. One of the shields of the air temperature sensors seen from the top.

Figure 3.4. The strings on which the shielded air temperature sensors are mounted.

3.2.2. Surface temperature sensors

Surface temperatures sensors are located on each of the four walls, at the ceiling and beneath the insulation of the floor of each test room. Figure 3.5 shows a surface temperature sensor mounted on the wall, while figure 3.6 shows the installation of a temperature sensor underneath the insulation on the floor.

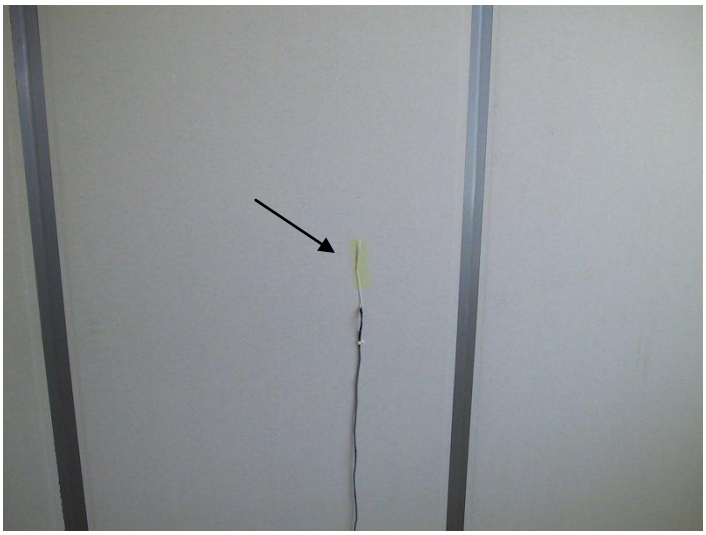

Figure 3.5. A surface temperature sensor at the wall.

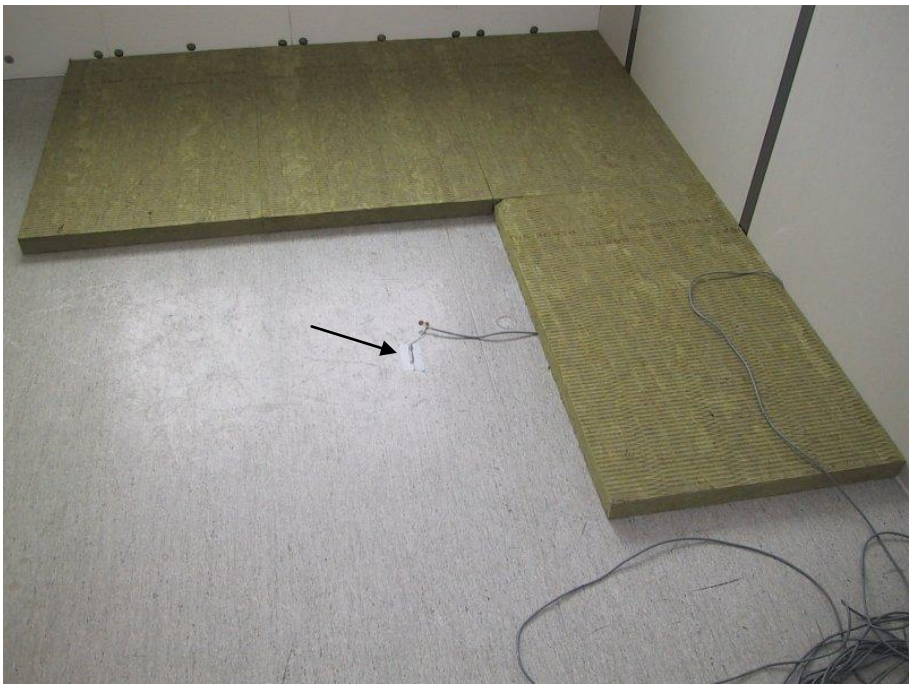

Figure 3.6. Temperature sensor mounted on the floor before the installation of the insulation on top of the existing floor.

3.2.3. Air temperature sensors around the test rooms

Figure 3.1 shows that the following air temperature sensors are located around the room:

- a shielded ambient temperature sensor – figure 3.7
- a (shielded) temperature sensor to the East and to the West of the test rooms in the surrounding laboratories – figure 3.8
- a temperature sensor to the north of the test rooms in the laboratory – figure 3.9
- one temperature sensor above each test room – figure 3.10

Figure 3.7. Shielded ambient temperature sensor on the column between the two test rooms. Shielded by two concentric cylinders as the air temperature sensors in the test room.

Figure 3.8. The shielded air temperature sensor in the laboratory to the West of the test rooms.

Figure 3.9. The air temperature sensor in the laboratory to the North of the test rooms.

Figure 3.10. One of the air temperature sensors above the test rooms.

3.2.4. Alarm temperature sensors

Figure 2.18 shows that each room is equipped with a water filled radiator. These radiators are covered with the 50 mm insulation foam on the inside of the external wall – see figure 2.19. The radiators are not functioning but it was not possible to empty them for water. However, the temperature of the air surrounding may possibly drop below 0°C at very low ambient temperatures. So in order to prevent damage due to freezing a temperature sensor is located at each radiator – figure 3.11. The data logger system is programmed to send an alarm via sms if one of the two alarm temperatures drops below a predefined temperature e.g. 5°C.

Figure 3.11 shows that a small part of the internal foam insulation can be removed in order to get into the temperatures sensors and to open for the radiation in order to prevent damage due to freezing. The holes are closed by pieces of insulation foam and sealed by means of tape.

3.2.5. Horizontal pyranometers

It is for the simulation model very important to know the split of the solar radiation between direct and diffuse radiation. This is measured using two calibrated pyranometers located on the roof of the building with the test rooms – see figure 3.12. The pyranometers are both calibrated pyranometers from Kipp & Zonen. One pyranometer (type CM 5) measures the global radiation, while the other (type CM 11) has a shading ring in order to measure the diffuse radiation. The shading ring of course shades not only the direct radiation but also part of the diffuse radiation. This is accounted for using the equations in (Battles et al, 1995). Having the global and diffuse horizontal radiation and knowing the incidence angle of the direct sun beam, the solar radiation on the façade can be calculated – this is described in details in Appendix A.

Figure 3.11. Temperature sensor for the alarm.

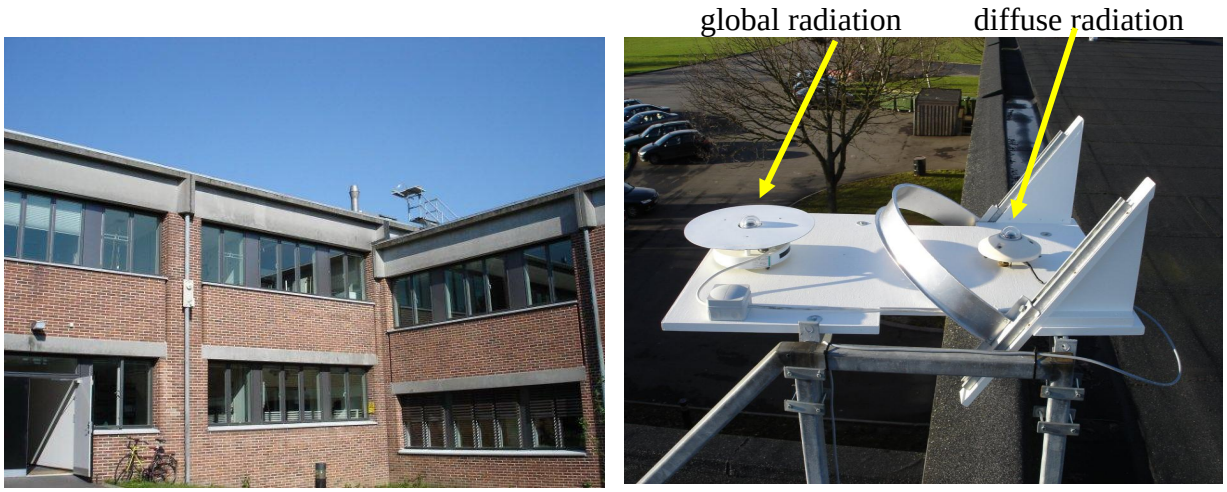

Figure 3.12. The pyranometers for measuring global and horizontal diffuse radiation.

3.2.6. Vertical pyranometers

Figure 3.13 shows the vertical pyranometer located between and under the windows of the test room. The purpose of this pyranometer is to measure the solar radiation hitting the windows of the test rooms. The pyranometer is a calibrated CM11 from Kipp & Zonen.

In order to determine the solar radiation transmitted through the glazing of the two test rooms a pv pyranometer (type 80SP from Soldata) was mounted in each of the open able windows of the two test rooms – see figure 3.14. The two pyranometers were calibrated with open windows using the calibrated external vertical pyranometer – see chapter 4.

The dimension of the pv sensor of the pyranometer is 49 x 49 mm² and is thus suitable to integrating the solar radiation coming through semitransparent glazing with patterns having a smaller dimension than the pyranometer.

Figure 3.13. The vertical external pyranometer.

Figure 3.14. The vertical internal pyranometers

During 2007 it was, however, discovered that the 80SPs gave wrong readings on the incoming solar radiation – se section 4.2. They were, therefore, calibrated using a calibrated pyranometer from Epply. And finally the Epply pyranometer was finally included in the measuring system for measuring the incoming solar radiation to test room A. Figure 3.15 shows a picture of the Epply pyranometer and the 80SP in test room A.

Figure 3.15. The Eppley and 80SP pyranometer in the window of test room A.

Early in 2008 MicroShades (like PowerShades but without pc cells) were installed in the windows of the laboratory with the test rooms. A pyranometer was therefore installed behind one of the windows as shown in figure 3.16. This pyranometer was a high precision CMP21 from Kipp & Zonen.

Figure 3.16. The CMP21 Kipp & Zonen pyranometer in one of the windows of laboratory

3.2.7. Lux meters

In order to determine the daylight in the test rooms a movable lux meter has been installed in each test room – see figure 3.17. The sensors are mounted on adjustable and movable tripods in order to ensure correct location of the sensors. The lux meters are Digital Light Meters from Extech model 401025. With one lux meter in the room and the other on the roof it is further possible to determine the daylight factor through the test rooms. The two lux meters give within < ±2% identical readings.

Figure 3.17. One of the two luxmeters. At the top installed on a adjustable and movable tri-pod. Bottom to the left: the instrument and bottom to the right the plane of the tripod with levels to insure horizontal location of the sensor.

3.2.8. Power meters

In order to be able to maintain a suitable temperature in the test room during the winter each test room is equipped with en electrical heater. In order to ensure good mixing of the air the heaters have a build in fan – the heaters are seen in figure 3.18.

In order to be able to compare the performance of the two test rooms under a heating regime it is mandatory to be able to measure the power consumption of the two heaters precisely. It was chosen to apply the SparOmeter power meter from NZN – the type with at serial port for communication. The power meter is shown in figure 3.19. The accuracy of the power meters is ±3 %.

Figure 3.18. One of the electrical heaters of the test rooms.

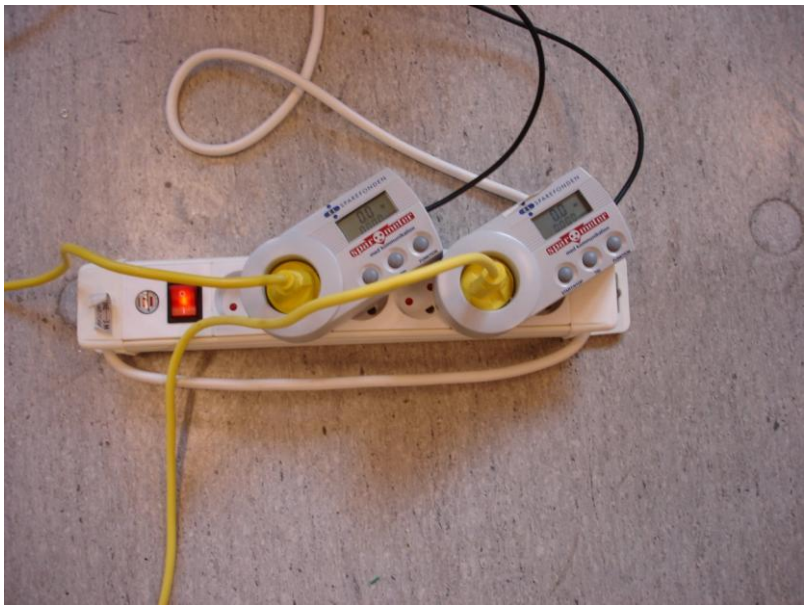

Figure 3.19. One of the power meters of the test romms.

3.3. Stabilization of the surrounding temperatures of the test romms

During 2007 it was discovered that there could be a rather high difference between the air temperature above the two test rooms and between the temperatures beside the two test rooms. To solve the first problem a small fan was located in the air space above each of the two test room in order to circulate air from the corridor behind the test room into the space above the test rooms – se figure 3.20. To solve the other problem the computer curtains of the room next to the laboratory with the test rooms were pulled down, and the measuring system

was enabled to control a small electrical heater in this room in order to obtain almost the same temperature as measured in the laboratory besides test room A. The electrical heater is shown in figure 3.21.

Figure 3.21. Fan for circulating the air above the test room.

Figure 3.21. Electrical heater for conditioning of the room next to test room B.

3.4. Data collection

All sensors are connected to a data logger system with modules from Analog Devices. The sensors are scanned each 5th second and averaged into five minuets values and stored on the hard disk of a pc.

The pc controlled via the software Labview 8.0 the data logger system. Spot values of the sensor readings together with curves showing several hours of measurements for some values are continuously shown on the screen of the pc. The data logger system is seen in figure 3.22.

Figure 3.22. The data logger system.

Using the data logger system/pc the measured values are directly transferred into physical understandable values like temperature, solar radiation and lux.

4. Calibration

In order to be able to perform side-by-side comparison and to calibrate a computer model of the test rooms it is essential that the obtained measuring data are of high quality with low uncertainty. The sensors incl. measuring system have, therefore, been exposed to several calibration procedures.

4.1. Temperature sensors

All temperature sensors are PT100 1/3 class B tested by the manufacture to have an accuracy of at least ±0.1 K at 0°C and ±0.27 K at 100°C.

The modules measuring the temperatures were calibrated using high precision resistances.

Figures 4.1-2 shows the 10 air temperatures in each room during a sunny day in September 2006 (September 12) with the original windows in both test rooms. The measured temperatures are almost identical during the night – a difference of less than 0.5 K, which is not far from the uncertainty of the sensors. During the day the difference is up to around 1 K due to the temperature stratification created by the sun. The observed bulks for some of the sensors during the day are due to the fact that the sun is heating the floor directly underneath the actual sensor, which therefore experience a temporary higher air temperature. No other out layers are observed.

Based on the calibration and the study of the actually obtained temperatures it is judge that the temperature measurements are of high quality.

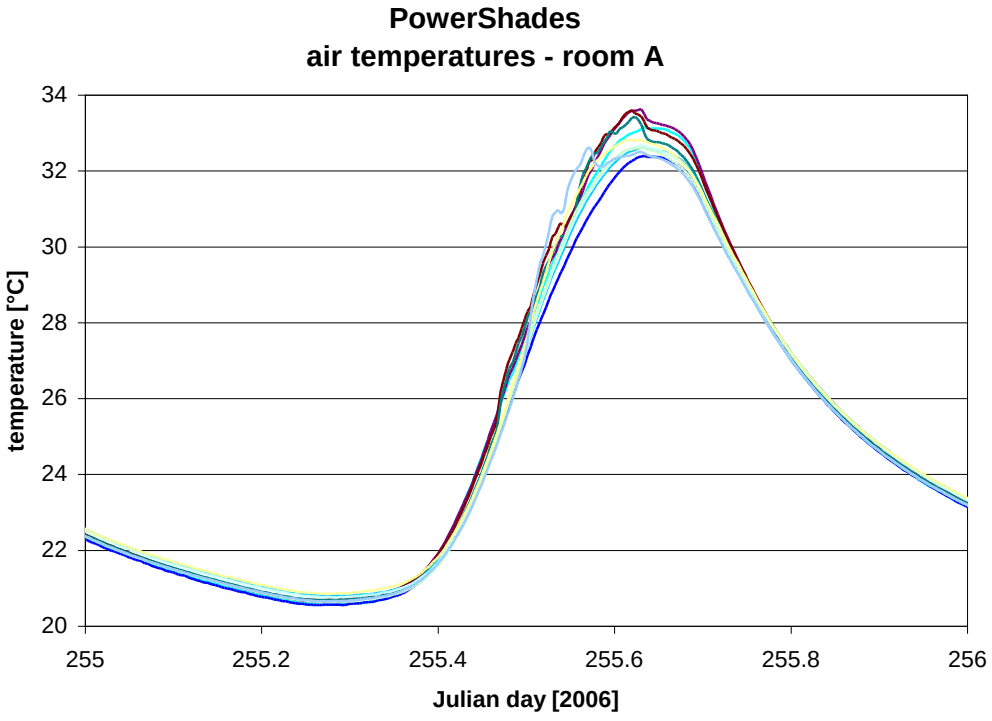

Figure 4.1. All 10 air temperatures in room A – September 12, 2006.

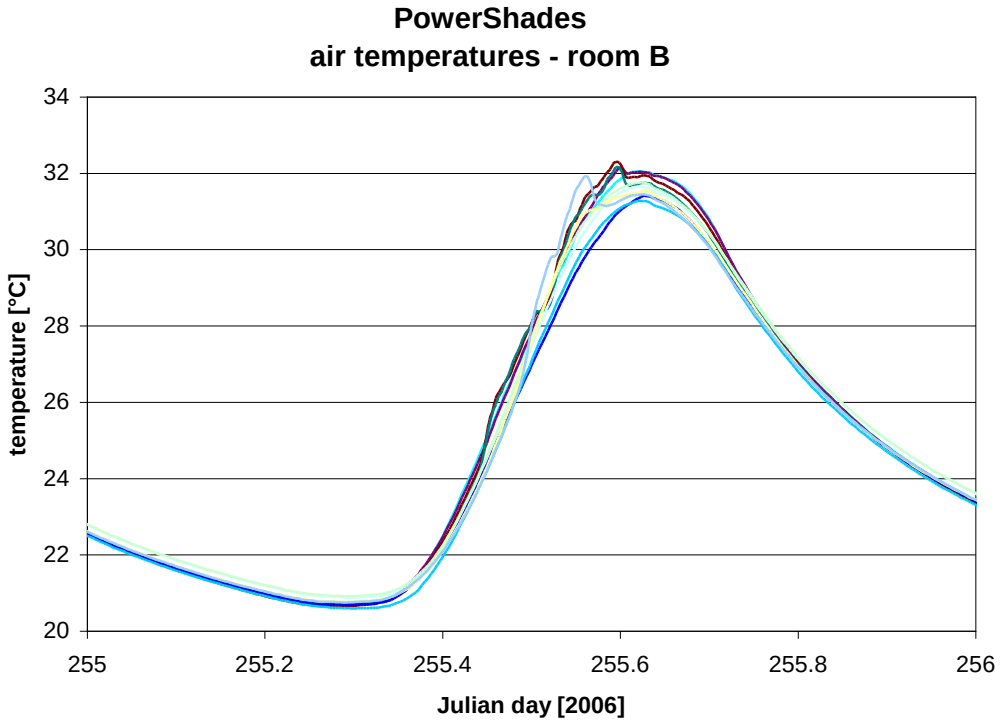

Figure 4.2. All 10 air temperatures in room B – September 12, 2006.

However, figures 4.1-2 also show that the temperature level of test room A around noon is about 1 K higher than in test room B. This is shown more clearly in figure 4.3. Figure 4.3 shows 7 days in September 2006 (September 12-18), which as seen in figure 4.4 was a sunny and warm period.

Figure 4.3 shows that there is a good match between the two mean air temperatures during the nights and during periods with low solar radiation, while there is a difference between 0,5-1,3 K during periods with high solar radiation. Later it is shown that the solar radiation to the two rooms are identical during main part of the day – except for some differences regarding shading during the morning and evening.

Except for being inverted the main differences between the two test cells is the wall of room B facing the room next to the laboratory containing the two test cells – se figure 2.2. This wall has two layers of gypsum plates and less insulation than the rest of the internal walls of the test rooms. This effect may be evaluated using the model of the test rooms developed in the simulation program ESP-r (ESRU, 2001). This evaluation can however, not be done for the period shown in figure 4.3-4 as the solar measuring station for measuring global and horizontal diffuse radiation was not installed during this period. Instead a period in March 2007 (March 22-28) with almost the same solar height as for figure 4.3-4 was chosen. The weather conditions for this period are shown in figure 4.5. Figure 4.6 shows the results from two runs of the models of the test rooms. The black curve is the result with room B as it is (two gypsum plates in on wall), while the red curve shows the result of removing one of the internal gypsum plates on the wall with two gypsum plates. It is seen that the extra gypsum plates reduces the mean air temperature with approx 0.5 K.

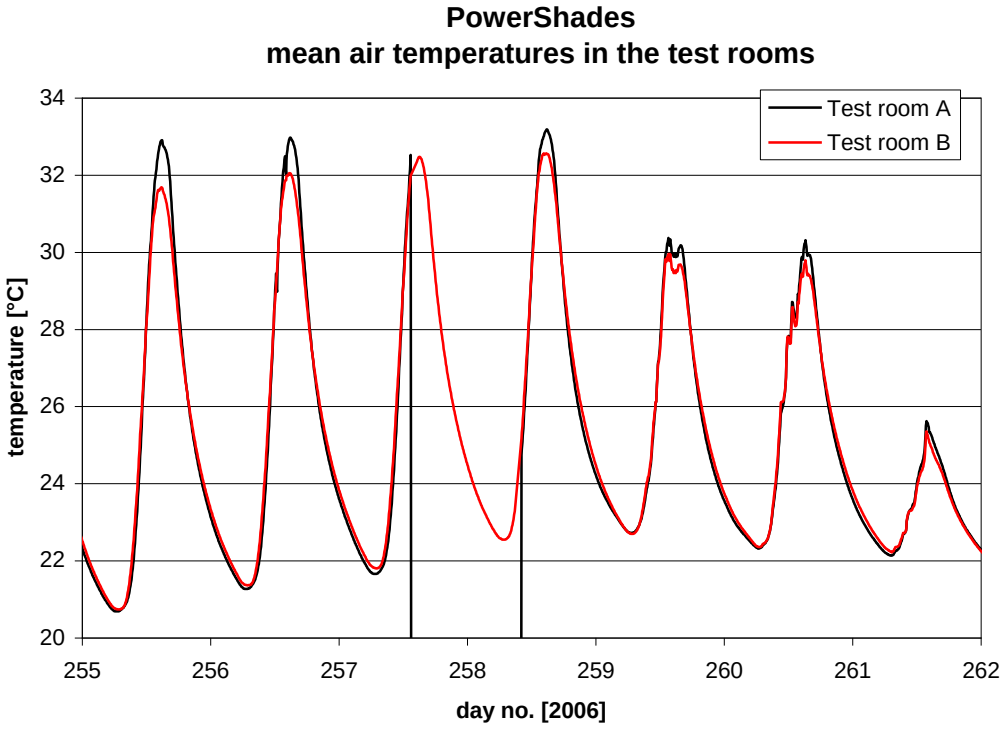

Figure 4.3. The mean air temperature of the two test rooms – September 12-18, 2006. There were unfortunately losses of data for room A for a period of approx. one day.

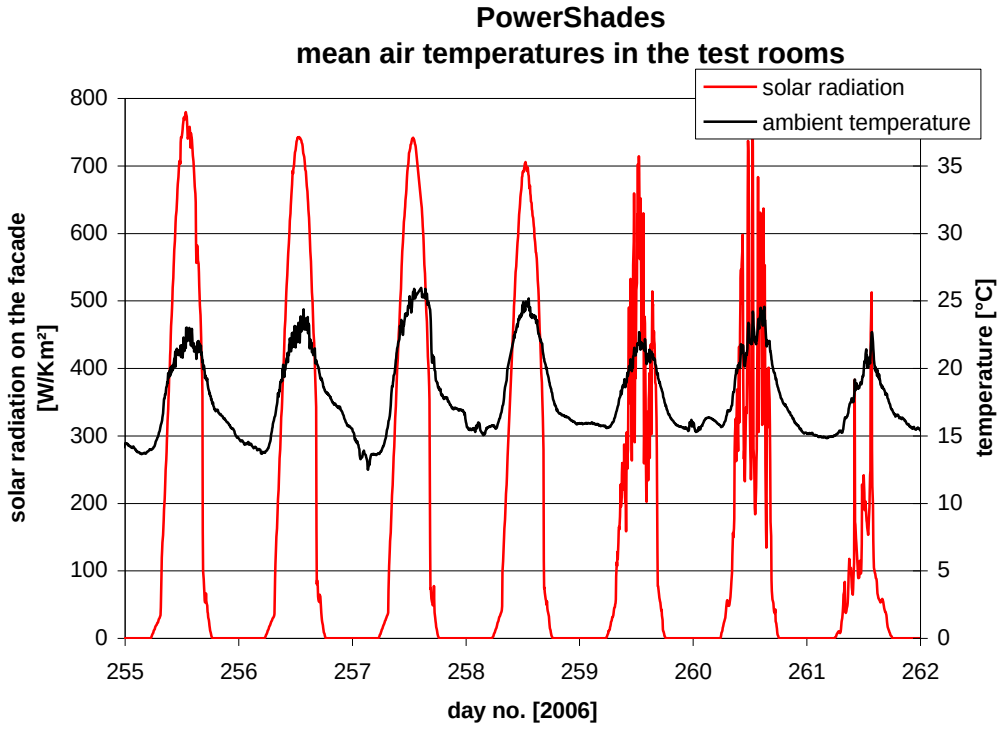

Figure 4.4. The ambient temperature and solar radiation on the façade – September 12-18, 2006.

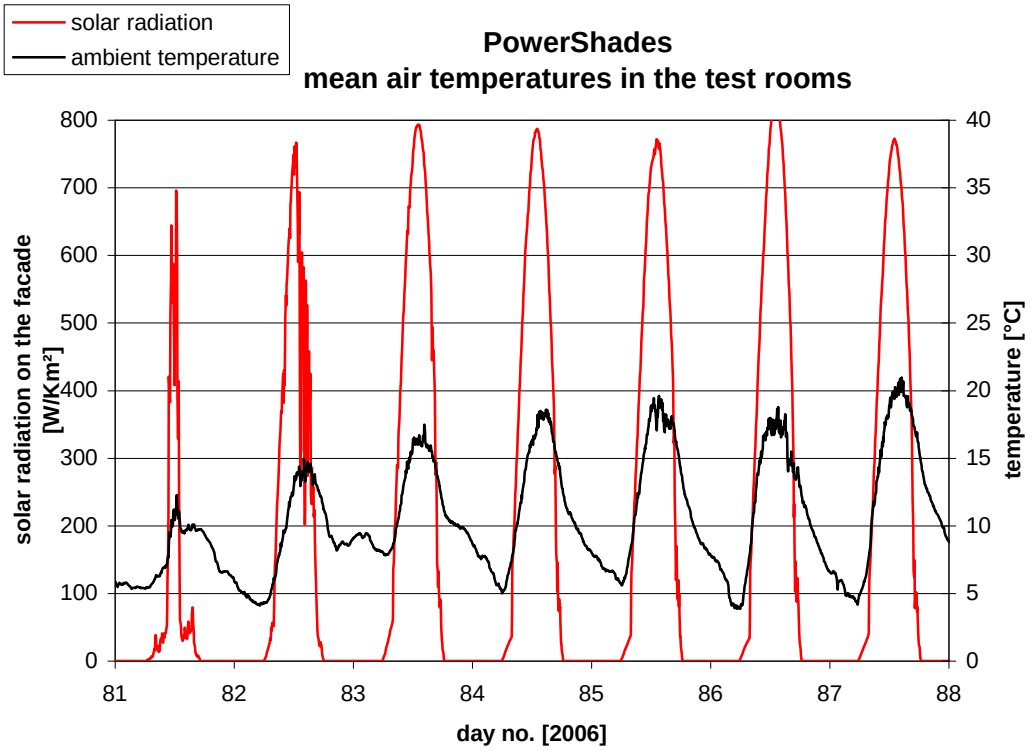

Figure 4.5. The ambient temperature and solar radiation on the façade – March 22-28, 2007.

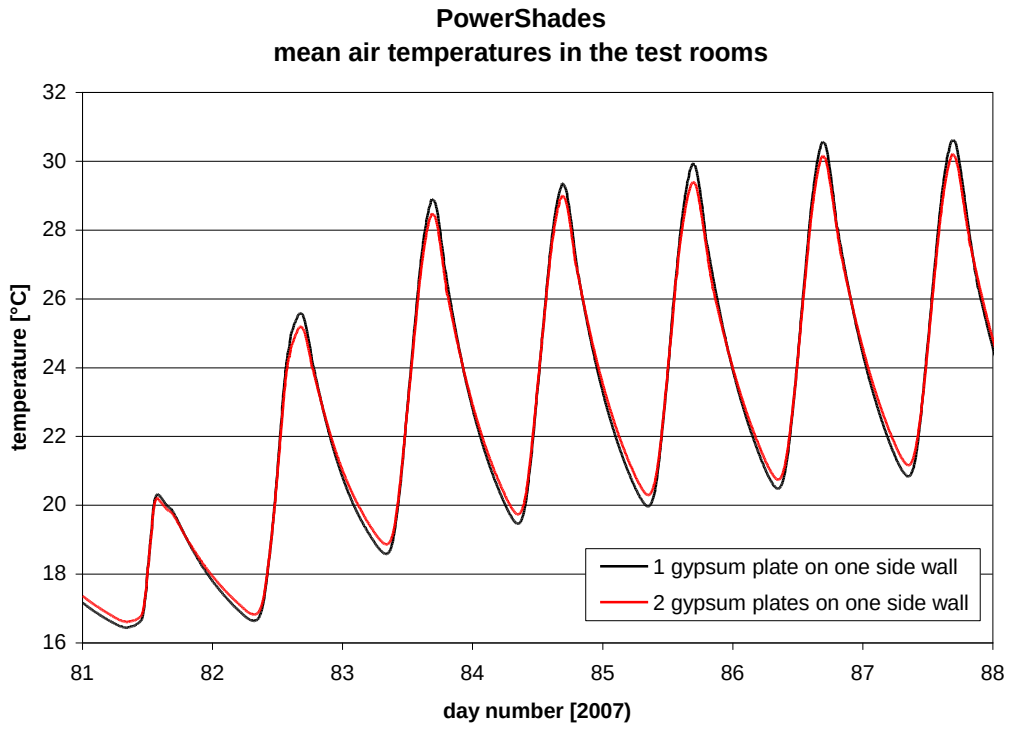

Figure 4.6. The mean air temperature of test room B simulated with one and two gypsum plates one on of the internal walls of test room B – March 22-28, 2007.

Figure 4.6 explains part of the difference shown in figure 4.3. Another problem with the wall between test room B and the room next to the laboratory with the test rooms is the insulation in the wall. The gap between the gypsum plates is 70 mm but the tightness of the insulation is only 50 mm. In the table on page 26 the conductivity of the insulation in this wall is estimated to be 0.74 W/mK assuming that the insulation is well mounted within the wall. However, figure 2.11 shows that the insulation may not be as precisely located as in the other walls. This may increase the conductivity of the insulation by e.g. 15% if convection in the air spaces occurs. Figure 4.7 shows the result of introducing this uncertainty in the model. The figure further shows the temperature of the room besides test room. Figure 4.7 shows that the introduction of a 15% higher conductivity of the insulation in the wall only have a minor influence on the air temperature in test room.

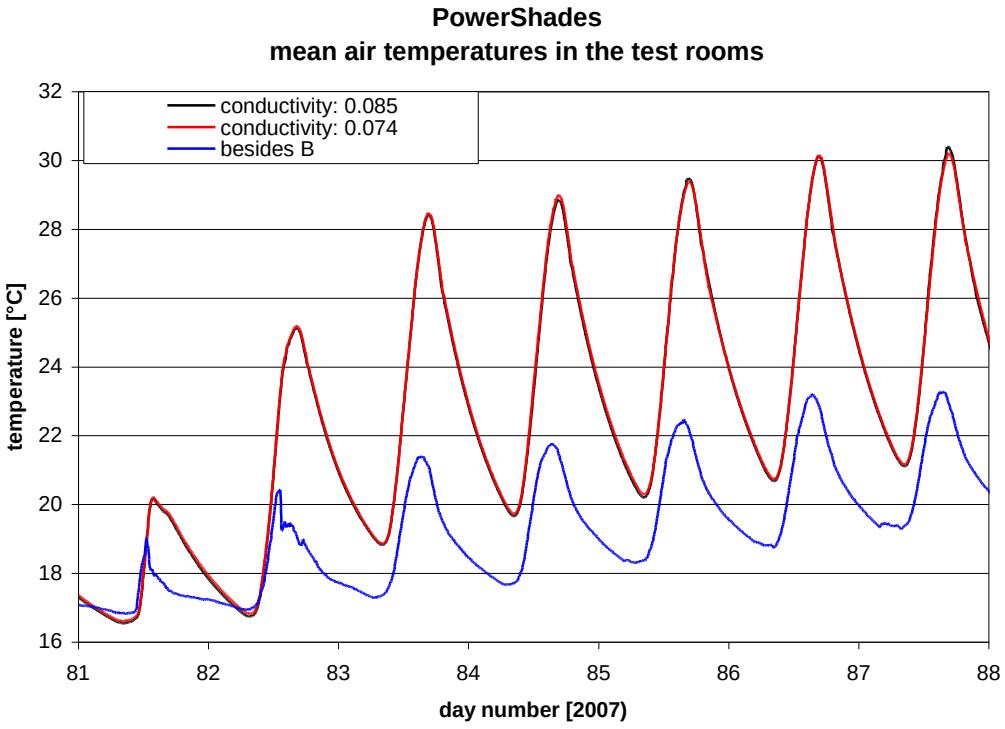

Figure 4.7. The mean air temperature of test room B simulated with a conductivity of 0,074 and 0,085 W/mK of the insulation in one of the internal walls of test room B – March 22-28, 2007. Besides B is the air temperature of the room adjacent to room B is shown.

Another difference between the two test rooms could be the glazing of the windows – ie that they did let in a different amount of solar radiation to the test rooms. However, at shown in the following section the two windows actually did let is the same amount of solar radiation. The only difference thus being differences in shading eg from the column between the two test rooms.

Based on the above it is judge that the two test rooms are fairly well matched with the exception of the extra gypsum plate on one of the walls in test room B. However, it has been shown that main part of the difference between the two test rooms may be accounted for using the model of the test rooms.

4.1.1. Surrounding temperatures

An effort has as described in section 3.3 been made in order to obtain matching surrounding temperatures for the two test cells. Figure 4.8-10 show these temperatures for an arbitrary chosen period in January-February 2008 (January28-February 3).

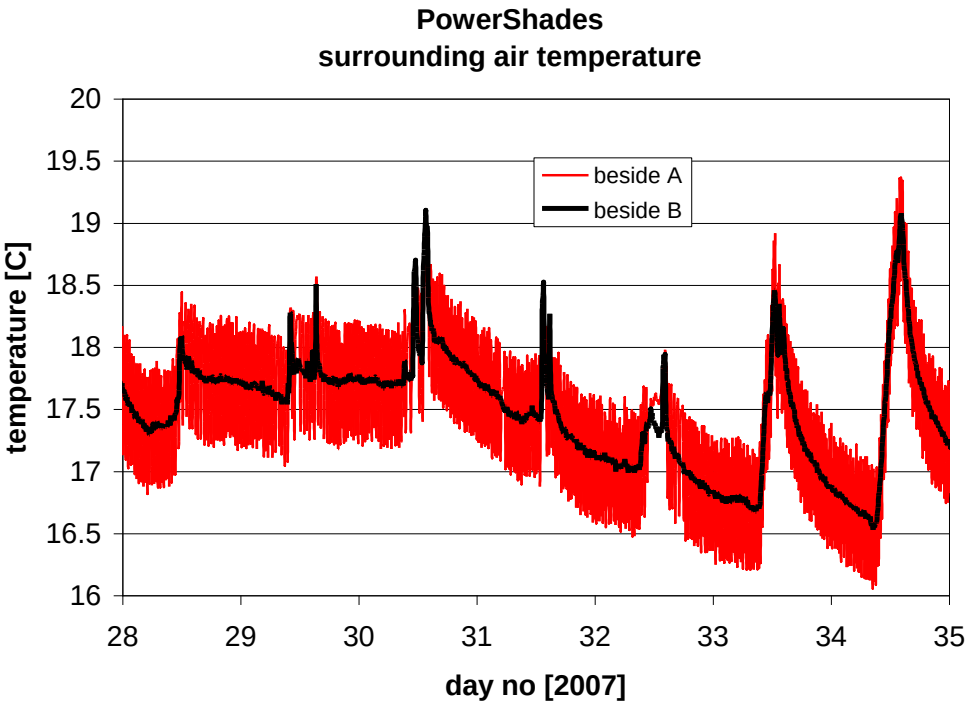

Figure 4.8. Air temperatures next to test room A and B - January28-February 3, 2008.

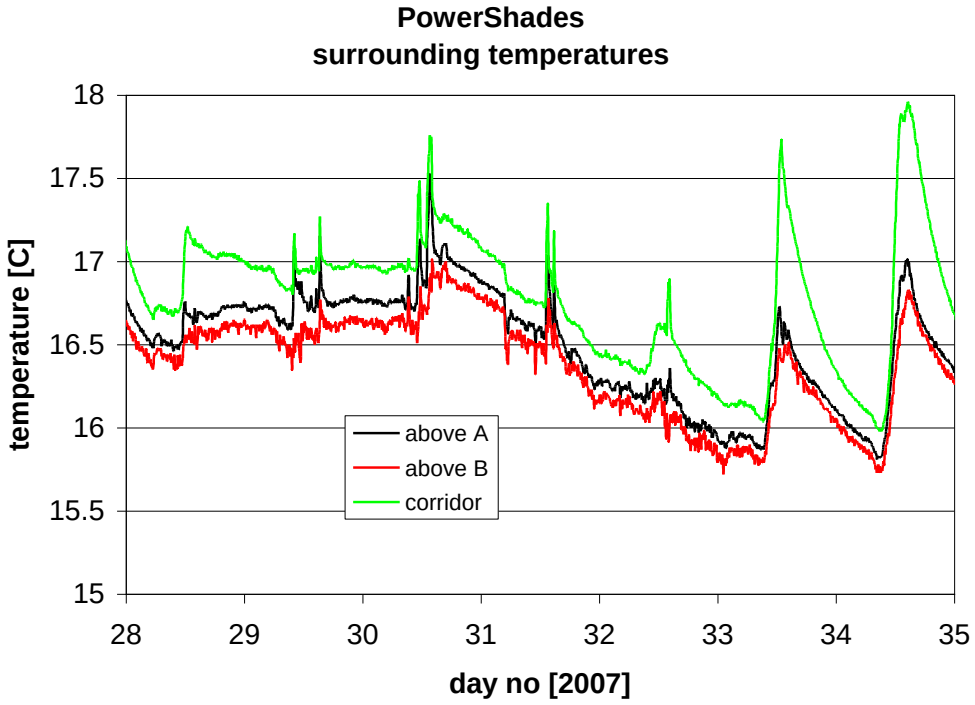

Figure 4.9. Air temperatures above and behind test room A and B - January28-February 3, 2008.

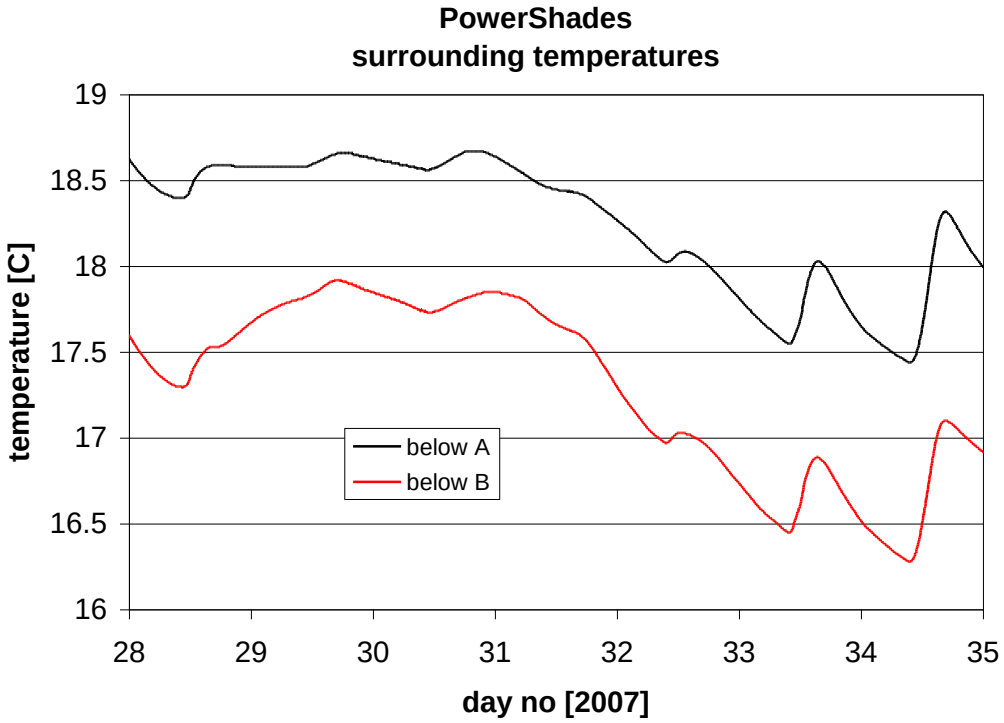

Figure 4.10. Temperatures below the insulation of the floor in test room A and B - January28-February 3, 2008.

Due to the hysteresis in the control of the electrical heater in the room next to test room B the air temperature of this room fluctuates around the temperature of the laboratory next to test room A – figure 4.8. However, for the shown period the mean temperature of the laboratory next to test room A was 14.093°C, while the mean air temperature of the room next to test room B was 14.084°C. So in mean these two temperatures are identical.

The temperatures above the test rooms are also very well matched. There is a difference of 1 K between the temperature below the insulation of the test rooms – due to different use of the offices below the test rooms. This temperature difference is however accounted for in the ESP-r model of the test rooms.

4.2. Solar radiation

All pyranometers have previously been exposed to traceable calibration. However, before installation the five original pyranometers they were mounted on the same plane and a side-by-side comparison were conducted. Within ±3% of actual reading the five pyranometers gave identical results.

After installation in-situ calibrations were further carried out.

4.2.1. Global and horizontal diffuse radiation

During the period September 26-October 25 the readings from the pyranometer measuring global radiation and diffuse horizontal radiation – the latter without shading ring – were compared – see figure 4.3 – with very good result. A better result can hardly be obtained.

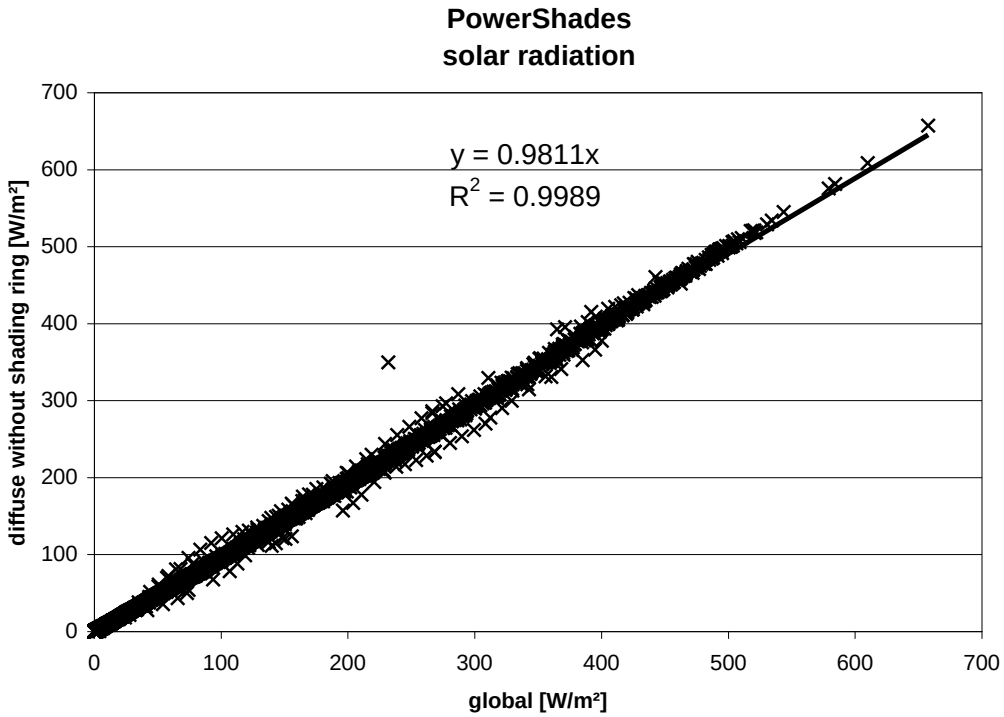

Figure 4.3. Comparison of readings from the pyranometer measuring the global radiation and the pyranometer measuring the diffuse horizontal radiation – the latter without shading ring.

The only way to investigate if the correction for the shading ring when calculating the diffuse radiation (Appendix A) is correct is to compare the calculated diffuse radiation with the readings from the pyranometer measuring the global radiation during overcast condition. This is done for December 23-30 in figure 4.4. An almost perfect match is obtained. A close up of day 364 is shown in figure 4.5 to show that there in fact two are curves in figure 4.4.

4.2.2. Vertical pyranometers

A side-by-side calibration of the three vertical mounted pyranometers was conducted. The two pv-pyranometers mounted behind the windows were compared to the external pyranometers – the latter has a traceable calibration. The comparison was conducted at noon with open windows on August 22, 2006 - a sunny day. The result is shown in figure 4.6.

Within less than ±3% identical readings were obtained. Figure 4.7 shows the measurements obtained from the three instruments on September 12, 2006. The original windows are here closed and the readings from the PV pyranometers have been corrected using the correction factors shown in figure 4.6.

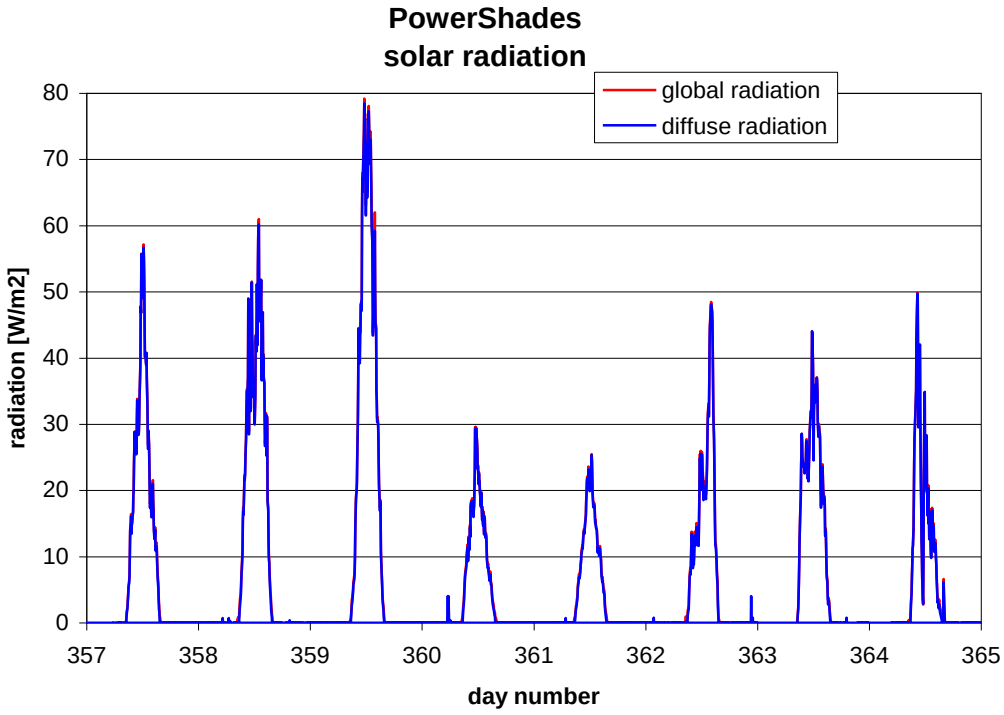

Figure 4.4. Comparison of the calculated diffuse radiation and the readings from the pyranometer measuring the global radiation during overcast conditions.

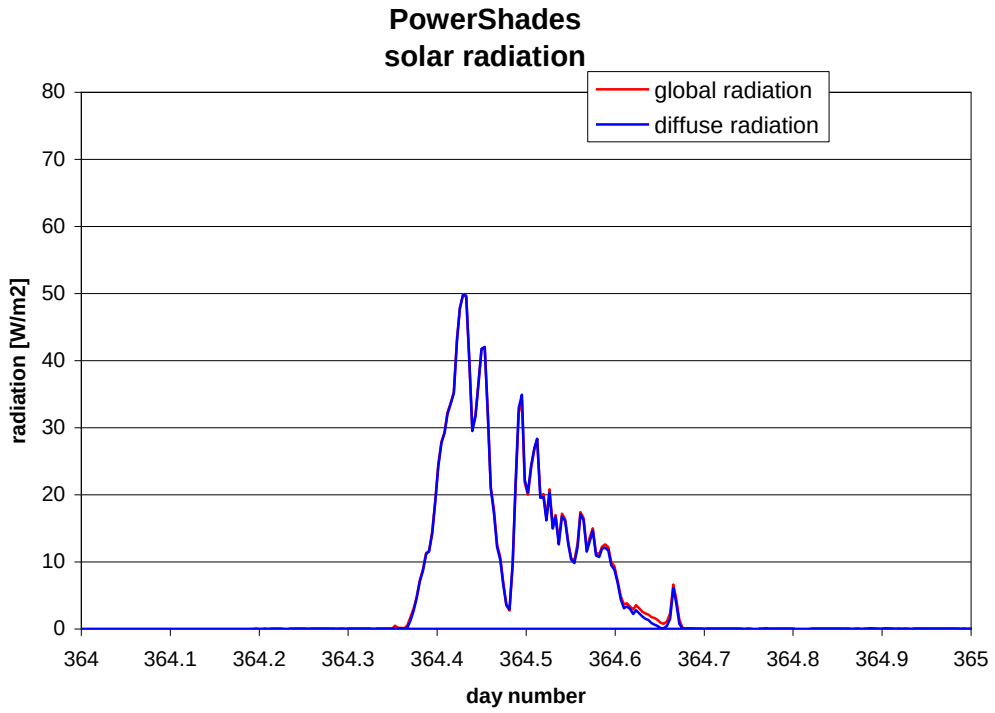

Figure 4.5. Comparison of the calculated diffuse radiation and the readings from the pyranometer measuring the global radiation during overcast conditions.

Figure 4.7 shows a well match between the two pyranometers located behind the glazing in the two rooms. The slower start in incoming radiation to room A in the morning is due to the column in the façade. It was expected to see a quicker drop for room B in the afternoon – also due to the column in the façade. However, the opposite is seen. The reason is a three to the right of the test cells which first shades the pyranometer in room A, then the external pyranometer and last the pyranometer in room B.

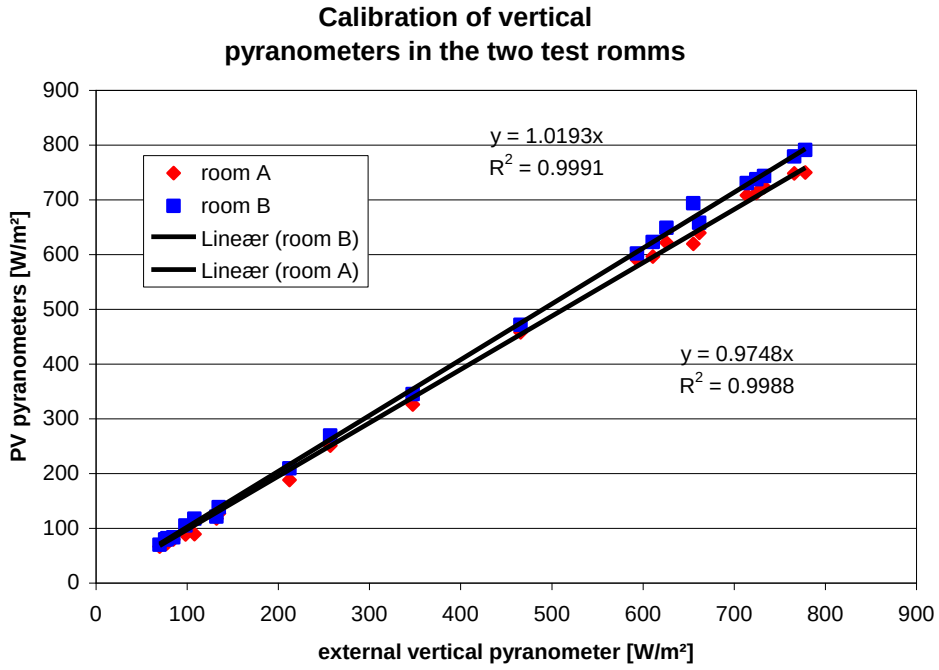

Figure 4.6. Comparison of the two PV pyranometers with the external vertical pyranometers at noon August 22 with open windows.

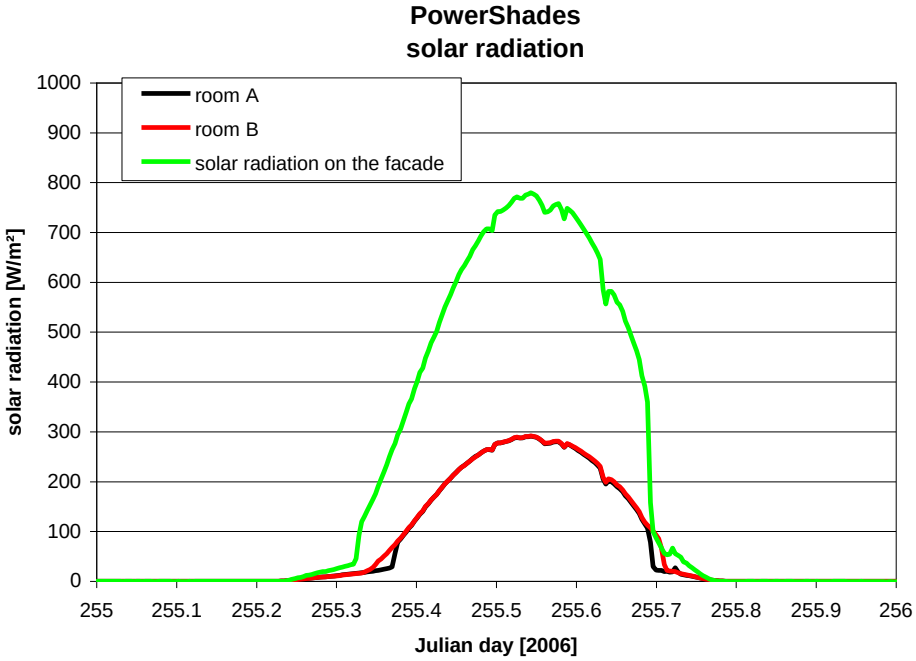

Figure 4.7. The solar radiation on the façade and behind the glazing of the two rooms – September 12.

However, a later comparison between the 80SP pyranometer behind a closed window and the Eppley pyranometer showed that the 80SP pyranometer had a too high reading as seen in figure 4.8. The reason for the too high reading behind the Velfac window is due to the fact, that the windows filter the incoming light differently for the different wavelengths of the solar radiation. The 80SP is only sensitive to solar radiation up to 1200 nm, while the Epplyes sensitivity is up to 3000 nm. So the calibration coefficient for the 80SP is not valid behind the window. However, a linier dependence between the 80SP and the Eppley is seen in figure 4.8. So the readings may easily be corrected by dividing with 1.17. The measurements from figure 4.7 for the incoming solar radiation to the two test rooms should thus be divided with 1.17. This, however, don't change the conclusions on this figure.

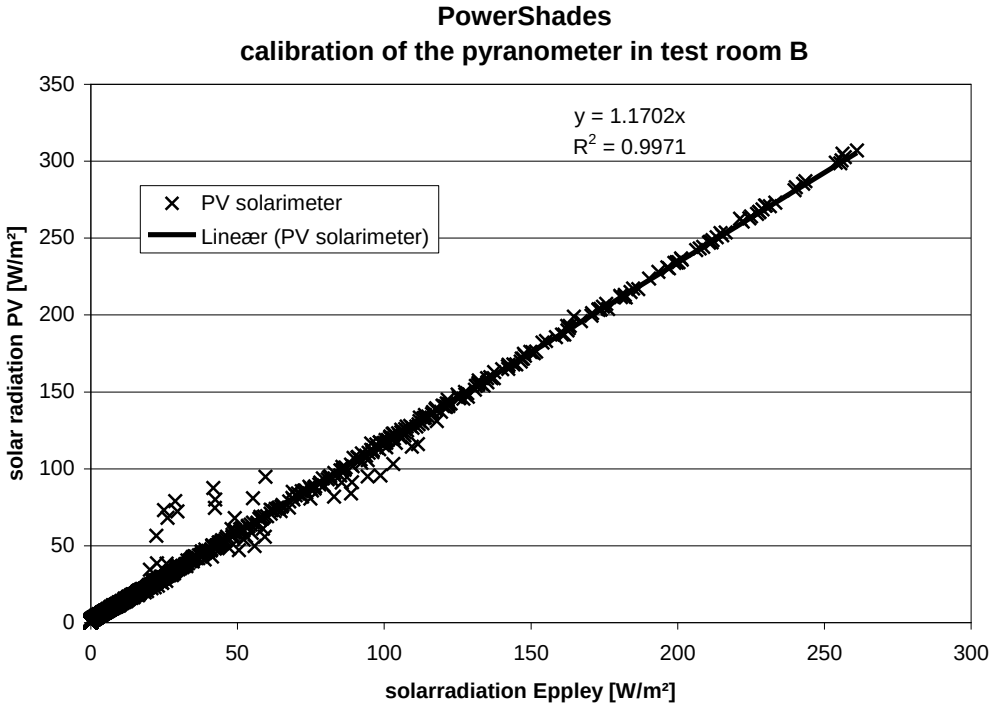

Figure 4.8. Calibration of the 80SP pyranometer behind the Velfac window.

The Epply and CMP21 pyranometers were calibrated by comparison with the vertical pyranometer on the façade, which has a traceable calibration record. The pyranometers were calibrated using data around noon with open window. The difference was as for the other pyranometers within ±3% of actual reading.

4.2.3. Conclusion

Based on the performed calibrations it is judged that the measurements from the pyranometers are of high quality.

4.3. Lux meters

The two lux meters are measuring the actual illumination in the test rooms but are also applied for obtaining daylight factors for the rooms – i.e. one lux meter is traversed through the room while the readings from this instrument is compared with the readings from the other lux meter situated on the roof of the building.

Only a side-by-side comparison has been conducted. The calibration by the manufacture for the absolute values is trusted. The absolute values are of less importance compared to the relative values which has been investigated by the side-by-side comparison.

Figure 4.9 shows a comparison for the whole range of the instruments while figure 4.10 shows a comparison in a range suitable for measuring in the rooms during overcast conditions. There is as seen a very good agreement between the readings from the two instruments.

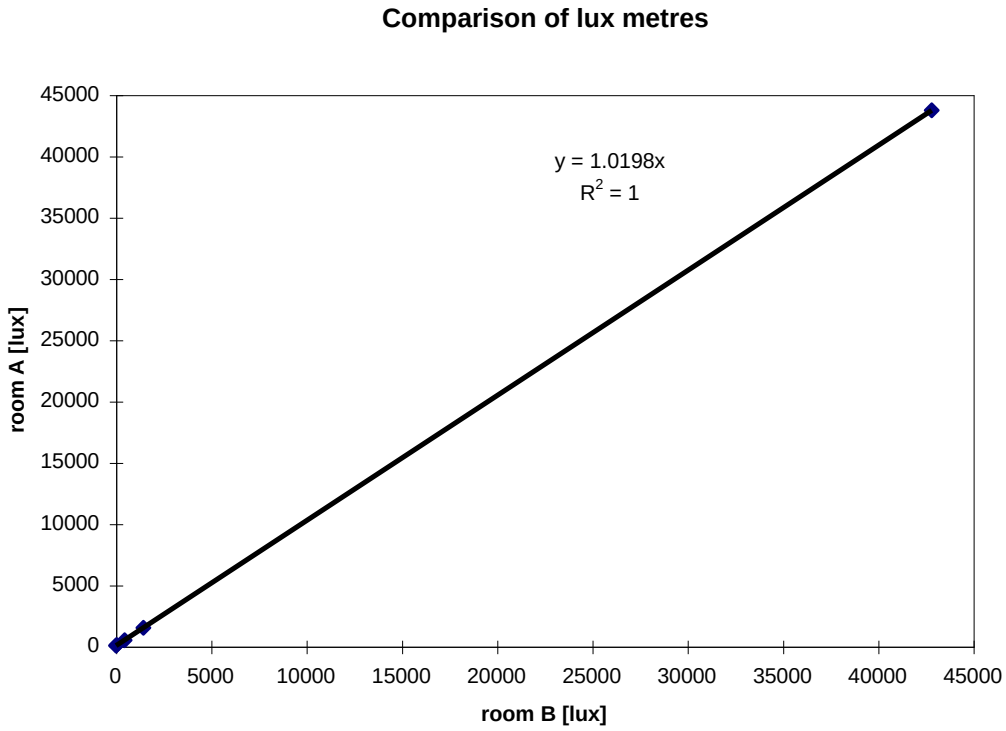

Figure 4.9. Full range comparison of the two lux metres.

Due to the mirroring of the test rooms the location of the lux meters has also been mirrored as seen in figure 4.11.

Figure 4.12 shows the illumination in the test rooms during September 6 – overcast conditions. Both rooms have the original windows. An almost perfect match is seen between the readings from the two instruments.

Figure 4.13 shows the illumination in the test rooms during a day with drifting clouds. Notice the different scale on the y-axis in figure 4.13 compared to figure 4.12. Due to different shading created by the column in the façade, the bars in the windows and the air temperature sen-

sors in the test rooms the pattern of the two curves is very different in the morning and in the afternoon as seen in figure 4.13. However, an almost perfect match is obtained around noon.

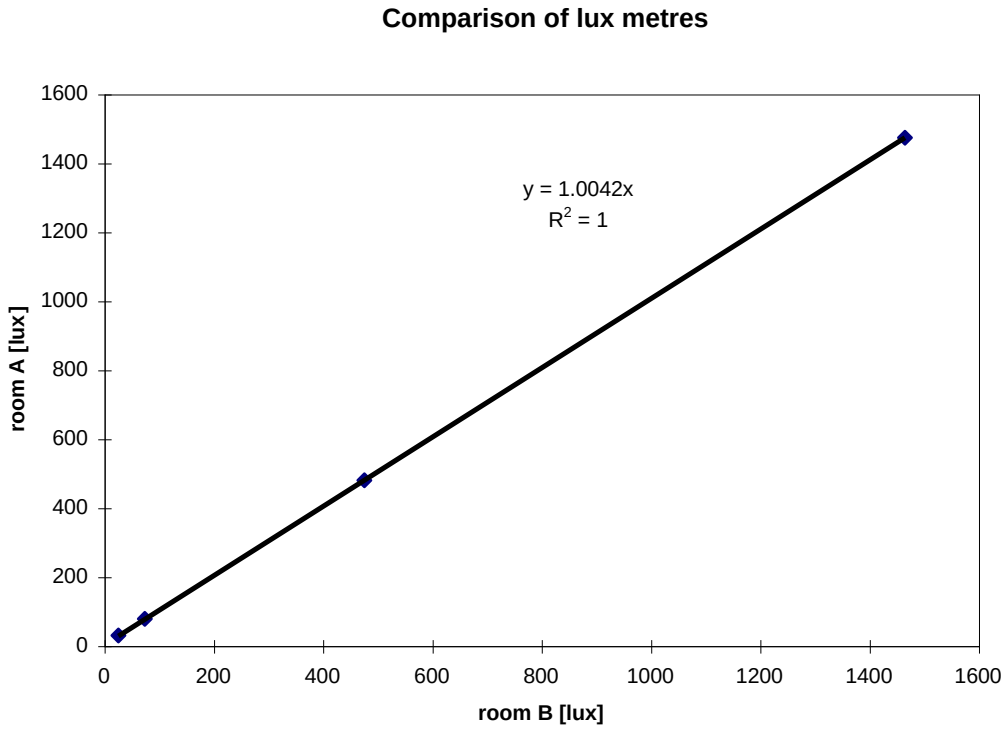

Figure 4.10. Comparison of the two lux metres at low lux levels.

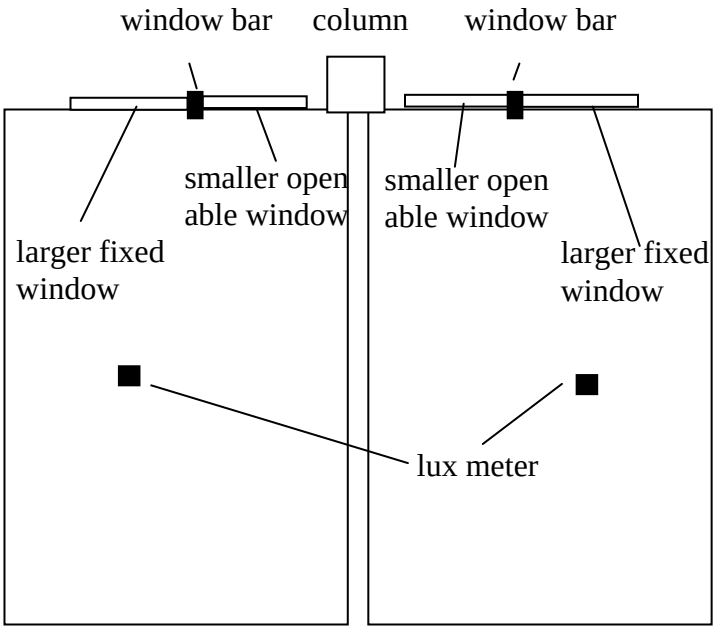

Figure 4.11. The mirroring of the two test cells.

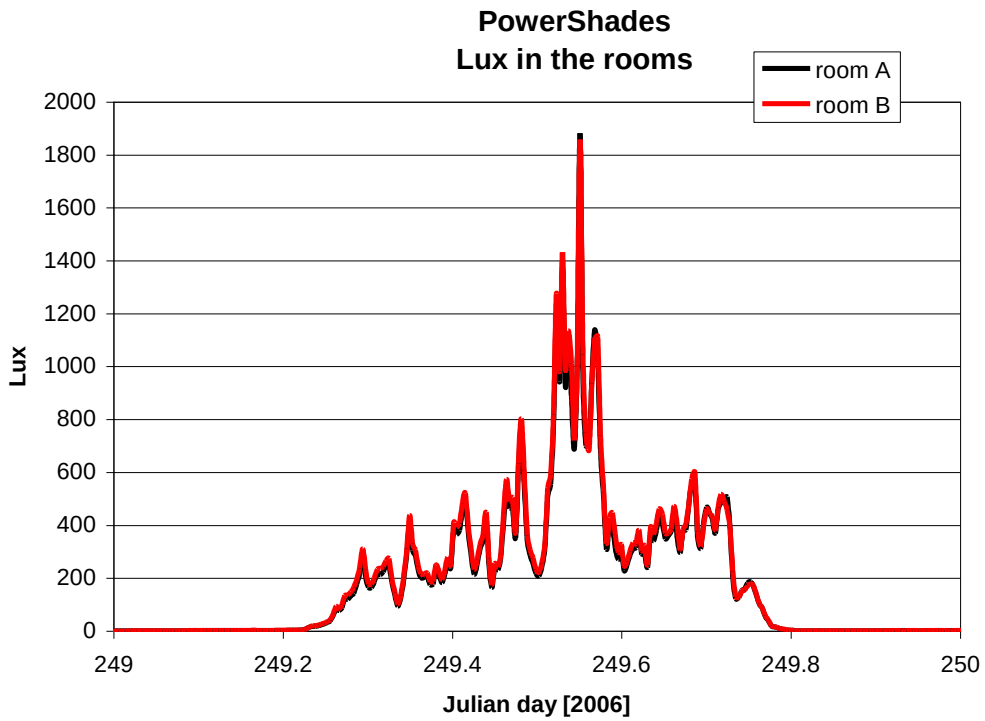

Figure 4.12. Illumination in the two test rooms – September 6.

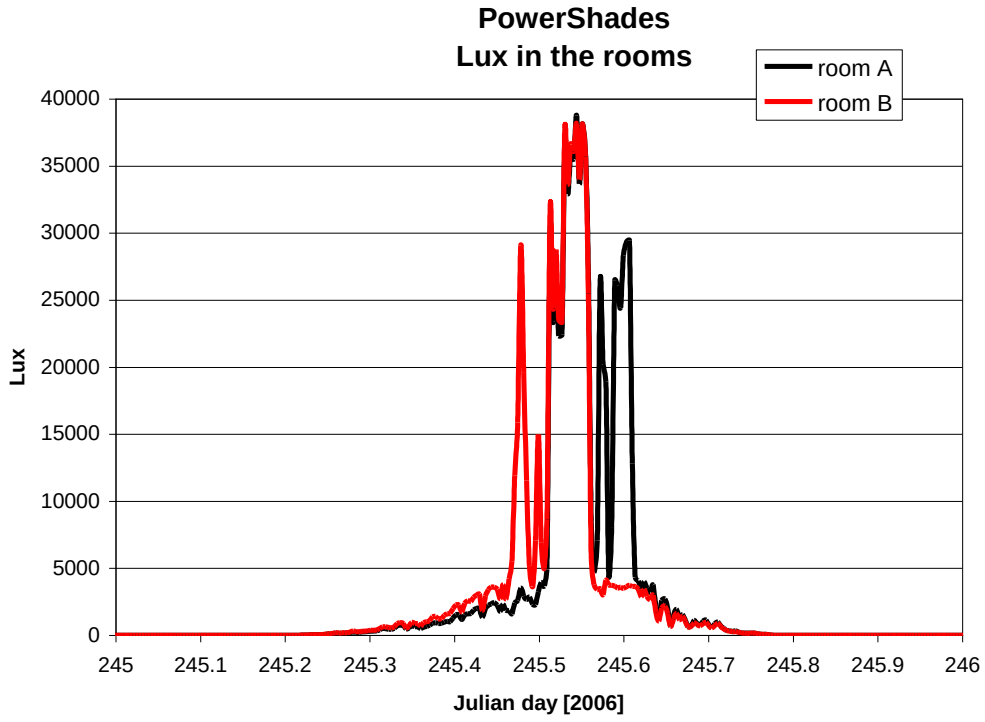

Figure 4.13. Illumination in the two test rooms – September 2.

Based of the above it is judged that the lux metres are well suited for the purpose and are obtaining high quality data.

5. References

Batlles. F.J. et al, 1995. On shadowband correction methods for diffuse irradiation measurements. Solar Energy, vol. 54, no. 2, pp. 105-114. Elsevier Science Ltd.

Bergsøe, N.C., 1992. Passiv sporgasmetode til ventilationsundersøgelser. The Danish Building Research Establishment. 1992. www.sbi.dk/indeklima/ventilation/ventilationsundersogelser-med-sporgas/?searchterm=sporgas

Dutre, W.L. A European Transient Simulation Model for Thermal Solar Systems – EMGP2. Solar Energy R&D in the European Community. Series A, volume 5. The Commission of the European Communities. 1985. ISBN 90-277-2051-7.

ESRU, 2001. Data Model Summary – ESP-r – Version 9 series. Energy Systems Research Unit, University of Strathclyde. December 2001.

Jensen et al, 1994. The PASSYS Project – Validation og Building Energy Simulation Programs – Part I and II. European Commission, Directorate-General XII for Science, Research and Development. February 1994. EUR 15115 EN.

Technological Institute, 2005. Transparent solar cells – the electricity producing solar shading of the future (in Danish). PEC Group, Technological Institute.

The SERC meteorological data base – volume II : algorithm manual. 2nd edition", Department of Building Science, University of Sheffield, UK

Appendix A: Calculation of the diffuse radiation

In the following is described how values for global, direct and diffuse radiation have been obtained.

Global radiation can easily be measured using calibrated pyranometer, while diffuse radiation can be measured using a pyranometer with a shading ring. Direct radiation is very difficult and expensive to measure. Direct radiation can instead be calculated based on global radiation and diffuse radiation on horizontal using the following equation:

$$G_b = (G_g - G_d)/\cos(v) \quad [1]$$

where: G_b is the direct radiation
G_g is the global radiation on horizontal
G_d is the diffuse radiation on horizontal
v is the incidence angle of the direct radiation on horizontal

Figure A.1 shows the instrumentation for measuring global and diffuse radiation.

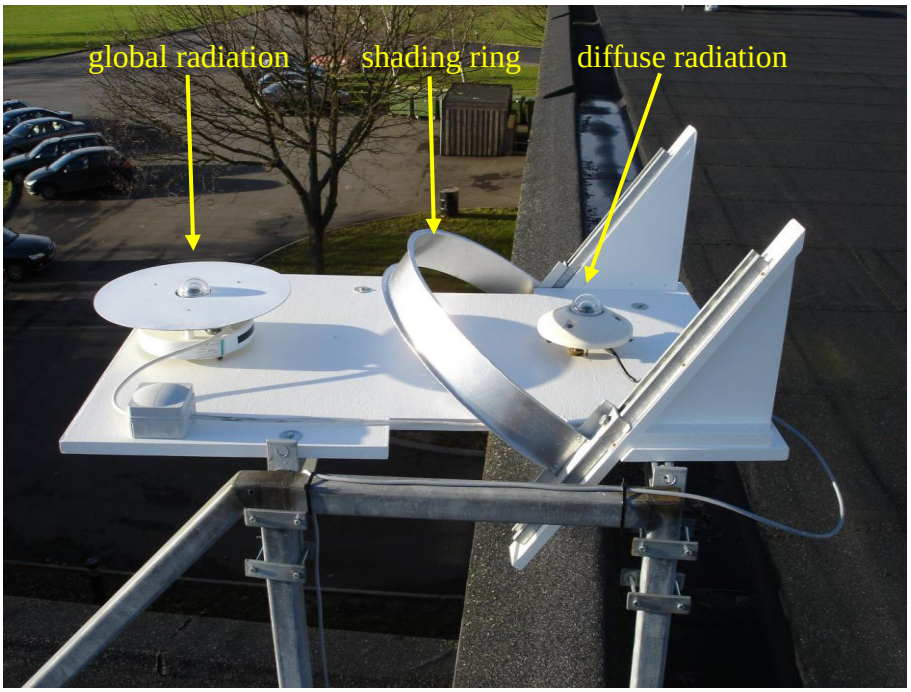

Figure A.1 The instrumentation for measuring global and diffuse horizontal radiation.

In order to measure the diffuse radiation the direct solar radiation has to be shades of from hitting the pyranometer measuring the diffuse radiation. This is done using a movable shading ring as seen in figure A.1 - with a radius of 0.275 m and a width of 0.07 m. The pyranometer is located in the centre of the half circle of the shading ring. The shading ring is parallel to south and tilted 55.4° towards south: a tilt equal to the latitude in order to always be able to screen off direct radiation.

However, the shading ring shades of more than the direct radiation. It also shades off part of the diffuse radiation. This has to be corrected for. For this correction is used the equation in

"On shadowband correction methods for diffuse irradiation measurements. Batlles, F.J. et al. Solar Energy, Vol. 54, no. 2, pp 105-114, 1995":

$$\Delta G_d = 2w / (\pi \cdot r) \cos^3\delta \, (\Psi_o \cdot \sin\phi \cdot \sin\delta + \cos\phi \cdot \cos\delta \cdot \sin\Psi_o) \quad [2]$$

where: ΔG_d is the faction of the diffuse radiation screened off by the shading ring
w is the width of the shading ring (here 0.07 m)
r is the radius of the shading ring (here 0.275 m)
δ is the solar declination
Ψ_o is the azimuth angle of the sun at sunset
ϕ is the latitude of the installation (here approx. 55.4°)

The solar declination may be found as (from "A European Transient Simulation Model for Thermal Solar Systems – EMGP2. Dutré, W.L. Solar Energy R&D in the European Community. Series A, volume 5. The Commission of the European Communities"):

$$\delta = 0.4092797 \sin (0.0172142 (n + 284)) \quad [3]$$

where: n is the number of the day (1, 2, 3, ….., 365)

The azimuth angle of the sun at sunset has been found using the program Almanak 1.0b VisualSoft Nakskov 1998 (in Danish) with the result shown in figure A.2. A regression line is also shown in the figure:

$$\Psi_o = 9.86 \cdot 10^{8} n^4 - 6.739 \cdot 10^{5} n^3 + 1.148 \cdot 10^{2} n^2 + 0.02152n + 48.467 \, [°] \quad [4]$$

where: n is the number of the day (1, 2, 3, ….., 365)

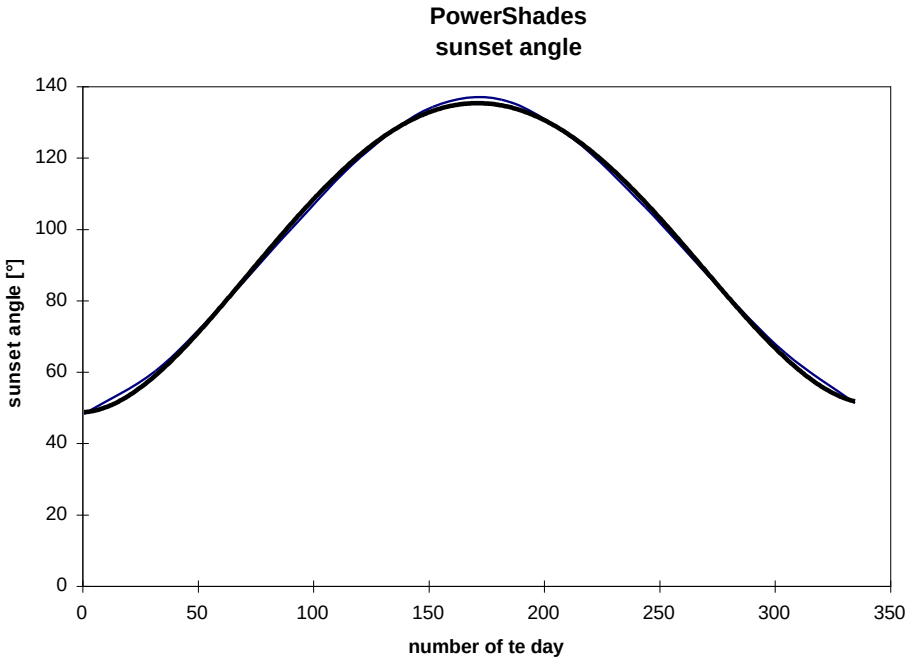

Figure A.2. The sunset angle over the year for the solar measuring station.

Figure A.3 shows the faction of the diffuse radiation screened off by the shading ring.

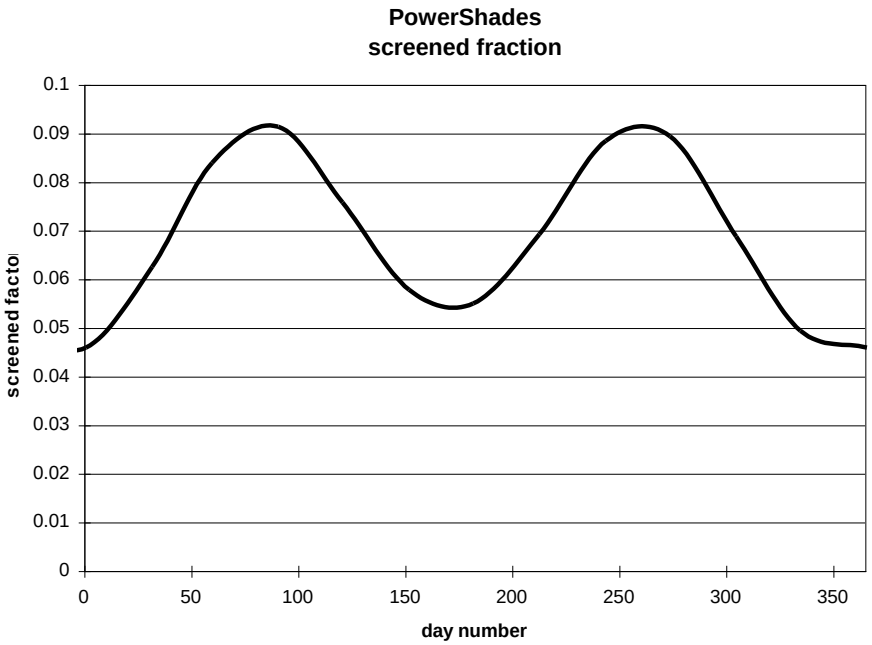

Figure A.3. The faction of the diffuse radiation screened off by the shading ring

The measured diffuse radiation should be corrected due to ΔG_d in the following was:

$$G_d = G_{dm} / (1- \Delta G_d) \quad [5]$$

where: G_d is the diffuse radiation
G_{dm} is the measured diffuse radiation not corrected for the shading ring
ΔG_d is the faction of the diffuse radiation screened off by the shading ring

The above correction for the shading ring is under the assumption that the sky is isotropic. However, there is a brighter area just around the sun called circum solar. In order to correct for this the following equation from "The SERC meteorological data base – volume II : algorithm manual. 2nd edition", Department of Building Sceince, University of Sheffield, UK, 1988 may be used:

$$f = 1.148 – 0.142 (G_{di} / G_g)^3 – 0.00118\delta \quad [6]$$

where: f is the correction factor for a non isotropic sky
G_{di} is the diffuse radiation with isotropic shading ring correction - eqn. [5]
G_g is the global radiation
δ is the solar declination

The shading factor for non isotropic sky is used in the following way:

$$G_d = f \cdot G_{di} \quad [7]$$

The above equations for correction of the measured diffuse radiation due to the shading ring have been implemented in a small program which automatically makes the correction to the measured diffuse radiation when handling the measured data.

Operation of the shading ring

In order to facilitate the operation of the shading ring, a scale has been mounted on each side of the track in which the shading ring slides – see figure A.4.

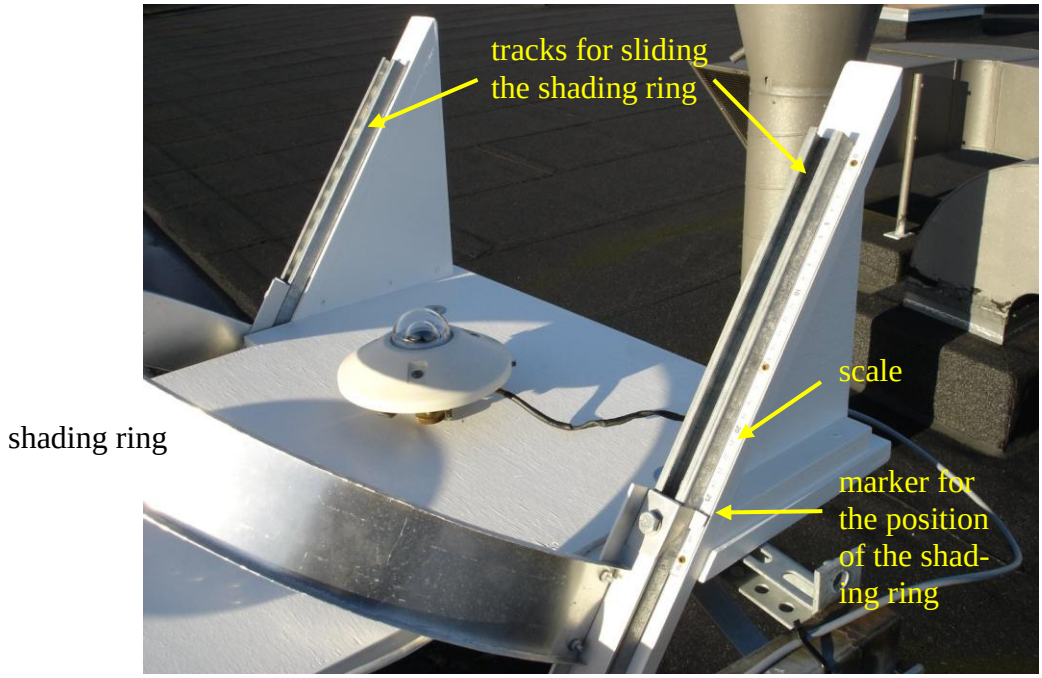

Figure A.4. Shading ring.

A marker (figure A.4) on each side of the shading ring gives the position of the shading ring. A curve for the position of the shading ring over the year has been generated and is shown in figure A.5.

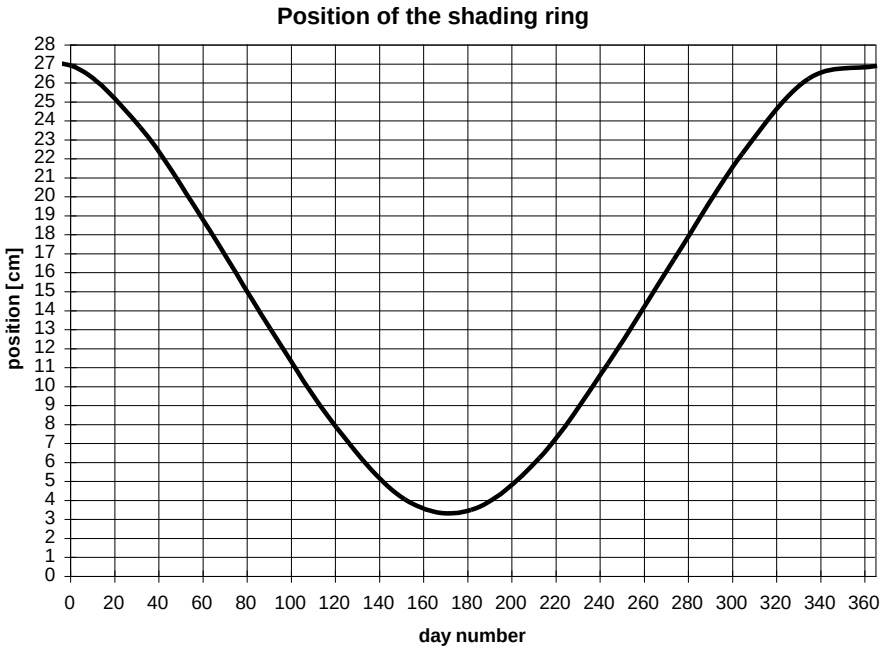

Figure A.5. Position of the shading ring.